Coordinatively Cross-Linked Binders for Silicon-Based Electrodes for Li-Ion Batteries: Beneficial Impact on Mechanical Properties and Electrochemical Performance

Lucas Huet, Driss Mazouzi, Philippe Moreau, Nicolas Dupré, Michael Paris, Sébastien Mittelette, Danielle Laurencin, Thomas Devic, Lionel Roué, Bernard Lestriez

Coordinatively Cross-linked Binders for Silicon-Based Electrodes for Li-ion Batteries: Beneficial Impact on Mechanical Properties and Electrochemical Performance

Lucas Huet,[a,b] *Driss Mazouzi,*[c] *Philippe Moreau,*[a] *Nicolas Dupré,*[a] *Michael Paris,*[a] *Sébastien Mittelette,*[d] *Danielle Laurencin,*[d] *Thomas Devic,*[a*] *Lionel Roué,*[b*] *Bernard Lestriez*[a]

[a] Nantes Université, CNRS, Institut des Matériaux de Nantes Jean Rouxel, IMN, Nantes F-44000, France.

[b] Institut National de la Recherche Scientifique (INRS), Centre Énergie, Matériaux, Télécommunications (EMT), Varennes, J3X 1S2, Canada.

[c] Materials, Natural Substances, Environment and Modeling Laboratory, Multidisciplinary Faculty of Taza, University of Sidi Mohamed Ben Abdellah, Fes, Morocco.

[d] ICGM, Université de Montpellier, CNRS, ENSCM, Montpellier, France.

* Corresponding authors: thomas.devic@cnrs-imn.fr; Lionel.Roue@inrs.ca

ABSTRACT

A simple and versatile preparation of Zn(II)-poly(carboxylates) reticulated binders by the addition of Zn(II) precursors ($ZnSO_4$, ZnO or $Zn(NO_3)_2$) into a pre-optimized poly(carboxylic acids) binder solution is proposed. These binders lead systematically to a significantly improved electrochemical performance when used for the formulation of silicon-based negative electrodes. The formation of carboxylate-Zn(II) coordination bonds formation is investigated by rheology, FTIR and NMR spectroscopies. Mechanical characterizations reveal that the coordinated binder offers a better electrode coating cohesion and adhesion to the current collector, as well as higher hardness and elastic modulus, which are even preserved in presence of a carbonate solvent (*i.e.* in battery operation conditions). Ultimately, as shown from *operando* dilatometry experiments, the electrode expansion during lithiation is reduced, mitigating electrode mechanical failure. Such coordinatively reticulated electrodes outperform their uncoordinated counterparts with an improved capacity retention of over 30% after 60 cycles.

KEYWORDS: *Li-ion batteries, silicon-based negative electrode, ionic cross-linked binder, Zn-carboxylate bonds.*

INTRODUCTION

The benefits and limitations of silicon as negative electrode material for lithium-ion batteries have already been clearly identified. The full lithiation of Si up to $Li_{15}Si_4$ leads to high gravimetric and volumetric theoretical capacities (approximately 3600 $mAh.g^{-1}$ and 2200 $mAh.cm^{-3}$, respectively), but it is associated with a substantial volume variation upon cycling (up to ~300%), giving rise to various failure mechanisms including silicon particles pulverization, loss of adhesion to the current collector, and solid electrolyte interphase (SEI) instability. Various strategies are explored to circumvent these issues. These are related to the active material optimization (*e.g.* Si nanostructuration, surface coating) and to the management of the electrode mechanical properties, especially through the binder optimization (which was thoroughly reviewed recently[1–4]).

Polar oxygenated polymers, such as polyacrylic acid (PAA), guar gum, alginate (Alg), carboxymethylcellulose (CMC), which can strongly interact with the Si particles surface, have been shown to outperform traditional binders such as polyvinylidene fluoride (PVDF). Strengthening the electrode through binder reticulation or cross-linking is another promising strategy.[5] Covalent organic cross-linking,[6] and more recently supramolecular cross-linking[7] (through ionic or hydrogen bonding, or even mechanical interlocking), are promising avenues, but they usually require specific tailor-made organic components. An alternative strategy relies on the formation of cation-ligand coordination bonds between the organic chains, also sometimes referred to as (metal) ionic cross-linking. Initially developed with Alg binders,[8–13] this strategy was recently extended to CMC,[14,15] to a catechol functionalized polymer,[16] and to an imidazole functionalized binder.[17] This method is easy to implement,

as it simply requires the addition of a metallic salt to an already established binder formulation with a polymer bearing complexing groups. We previously demonstrated this with CMC and copper sulfate.[15] Coordination bonds are also highly dynamic, hence potentially prone to sustain strong mechanical stresses and to induce self-healing properties in the electrodes.[18]

In the present study, attention is focused on a pre-optimized formulation comprised of CMC and citric acid (CA), which already lead to respectable electrochemical performance. Nevertheless, addition of Zn(II) precursors ($ZnSO_4$, ZnO or $Zn(NO_3)_2$) leads to a significant improvement in electrochemical performance, notably to the capacity retention. Such an improvement was also observed with the addition of $CuSO_4$ [15] and thus, one of the objectives of present study is to confirm that this strategy can be generalized to other metallic cations. Moreover, a combination of advanced characterization techniques is used for a better understanding of the binder properties. Information about the coordination of the carboxylic/carboxylate groups are obtained by a combination of IR and ^{1}H-^{13}C CP MAS NMR, pushing further the understanding of the binder behavior in terms of coordination with Zn cations within the composite electrode. In addition, to the best of our knowledge, it is the first time that ^{17}O MAS NMR is used to characterize the local environments formed by the mixing of CA and the CMC binder directly within a realistic electrode. The contribution of CA in the formation of the reticular network is also highlighted. We recently demonstrated that such a coordinated CMC/CA/Zn(II) binder act, at least partially, as an artificial SEI.[19] We here show that such bonds have also a beneficial impact on the electrode's mechanical properties in both the dry and carbonate solvent-soaked states as evidenced by scratch tests and nano-indentation experiments. The invariability of the mechanical properties (hardness and elastic modulus) of the crosslinked binder in the presence of the electrolyte, unlike the un-crosslinked binder, is also demonstrated.

Additionally, *operando* dilatometry experiments are performed to evaluate the impact of this mechanical strengthening on the electrode expansion/contraction upon cycling.

RESULTS AND DISCUSSION

Electrode composition and electrochemical performance.

Inks for electrode fabrication were prepared by mixing an aqueous binder solution with a given amount of silicon and conducting additive (graphene) to reach a final silicon/graphene/binder composition close to 70:10:20 $_w$% (see **Table 1**). The reference binder solution was already thoroughly studied by our research group in the last years (see [15] and the references therein). It consists of sodium carboxymethylcellulose (NaCMC) dissolved in a buffer solution of citric acid (CA) and sodium or potassium hydroxide, which is required to reach the desired pH of 3-3.5. As mentioned above, we already showed that the addition of Cu(II) lead to a noticeable improvement of the electrochemical performance.[15] The extension to diamagnetic Zn(II) present several advantages, including (i) the evidence that this approach can be generalized to different cations, (ii) the easy access to solid-state NMR spectroscopy, hardly available with paramagnetic Cu(II), and (iii) the possibility to distinguish cations coming from the binder and the corrosion of the Cu current collector. The effect of the addition of Zn(II) ions was evaluated together with the coordination ratio, *i.e.* the amount of Zn(II) *vs.* the total number of carboxylic groups (coming both from CMC and CA), and the nature of the metallic precursor ($ZnSO_4$, $Zn(NO_3)_2$ and ZnO). ZnO is particularly appealing as it considerably reduces the dead mass in the electrode, but its basic nature in acidic solutions leads to a significant pH increase (pH > 4). Therefore, another reference ink containing additional LiOH was prepared to reach a similar pH value as the ZnO solution (4.4 and 4.3, respectively). In regards to the coordination

ratio, Zn/RCO_2H = 0.22 and 0.66 were used since our previous study on Cu-CMC-CA coordination binder suggested that a ratio above 0.1 leads to optimal electrochemical performance.[15] **Table 1** summarizes the binder formulations used in this study, the corresponding ink solid fractions and pH, and the electrode compositions in wt%.

Table 1. *Binder formulations, corresponding electrode compositions, and ink properties.*

Formulation name		Electrode composition ($_w$%)						Ink property	
Salt	Coord. ratio	Silicon	Graphene	NaCMC	Citric acid	$KOH^{\circ}/NaOH^{\blacksquare}$ $(+LiOH)^{\lozenge}$	Zn precursor	Solid fraction ($_w$%)	pH
w/o	0	73.4	11.0	7.2	7.4	1°	0	21.5	3.5
$ZnSO_4$	0.66	63.7	9.6	6.2	6.4	0.9°	13.2	24.0	2.6
$ZnSO_4$	0.22	69.9	10.5	6.8	7.0	1°	4.8	22.3	2.9
$Zn(NO_3)_2$	0.22	69.3	10.4	6.8	6.9	1°	5.6	22.5	2.7
ZnO	0.22	71.8	10.8	7.0	7.2	$0.7^{\blacksquare}$	2.5	21.8	4.3
w/o + LiOH	0	73.1	11.0	7.2	7.3	$1.4^{\blacksquare\lozenge}$	0	21.5	4.4

For the electrochemical evaluations, electrodes with a Si mass loading equal to 1.75 $mg_{Si}.cm^{-2}$ were used. The specific discharge capacity per cycle (mean and standard deviation results from multiple cell tests, see **Table S1** in supporting information (SI)) is shown in **Figure 1a** for electrodes containing 0.22 and 0.66 equivalents of $ZnSO_4$ per carboxylic group (RCO_2H) (labeled $ZnSO_4$ (0.22) and $ZnSO_4$ (0.66), respectively) and the related zinc-free reference. Note that some variability between cells is inevitable for a same formulation (see error bars in **Figure 1** and cycling performance of individual cells in **Figure S1**). The main source of error comes from the weighting of the electrodes. Actually, a very small variation of the electrode weight (which may originate from a small variation of the Cu collector thickness) leads to an under or upper evaluation of the silicon loading, which then affects the specific capacity calculations. However, despite this variability, the better cycling performance of the Zn-containing electrodes is clearly demonstrated.

Regardless of the formulation, the initial discharge capacities are higher than the theoretical capacity (3580 $mAh.g_{Si}^{-1}$ considering the formation of $Li_{15}Si_4$). This excess capacity is of approximately 580, 520, and 330 $mAh.g_{Si}^{-1}$ for the reference, $ZnSO_4$ (0.22) and $ZnSO_4$ (0.66) electrodes, respectively. The graphene contribution is of approximately 50 $mAh.g_{Si}^{-1}$. This value is obtained by taking 350 $mAh.g^{-1}$ as the reversible capacity of the graphene additive [20,21]. Based on a previous study,[21] the contribution of the binder organic components is likely to be negligible. Specifically, no reduction peak at 1.6-1.7 V (*vs.* Li^+/Li^0), characteristic of the reduction of carboxylic acidic protons,[22,23] is detected on the dQ/dV curves (**Figure S2)**. Furthermore, the addition of Zn(II) cations does not lead to additional reduction peaks on these curves, indicating that the reduction of Zn(II) to Zn(0) does not occur, or only to a negligible extent. This is in full agreement with previous findings on Ni-Alg binder[24] and our own STEM-EDX analysis on cycled Zn-CMC-CA binder electrodes,[19] where no significant formation of metallic Zn particles was detected. Actually, even if the electroreduction of Zn(II) to Zn(0) occurred upon cycling, this extra capacity would be negligible (*e.g.*, 23 mAh g^{-1} Si for the $ZnSO_4$ (0.22) electrodes, see equation (1) in the SI) compared to that of Si (≈ 3600 mAh g^{-1} Si).

On the other hand, from our recent ^{7}Li NMR quantifications,[19] the amount of Li in the SEI (in the form of LiF, Li_xPO_yFz and other species) corresponds to an extra 345 and 373 $mAh.g_{Si}^{-1}$, for the $ZnSO_4$ (0.22) and its reference formulation, respectively (see equation (2) in the SI).[19] Therefore, both in the presence and absence of Zn(II), the electrolyte degradation is the major source of extra capacity. Interestingly, the latter is decreased for Zn-containing electrodes, in agreement with previous work which indicates that coordinated binder act, at least partially, as an artificial SEI.[19]

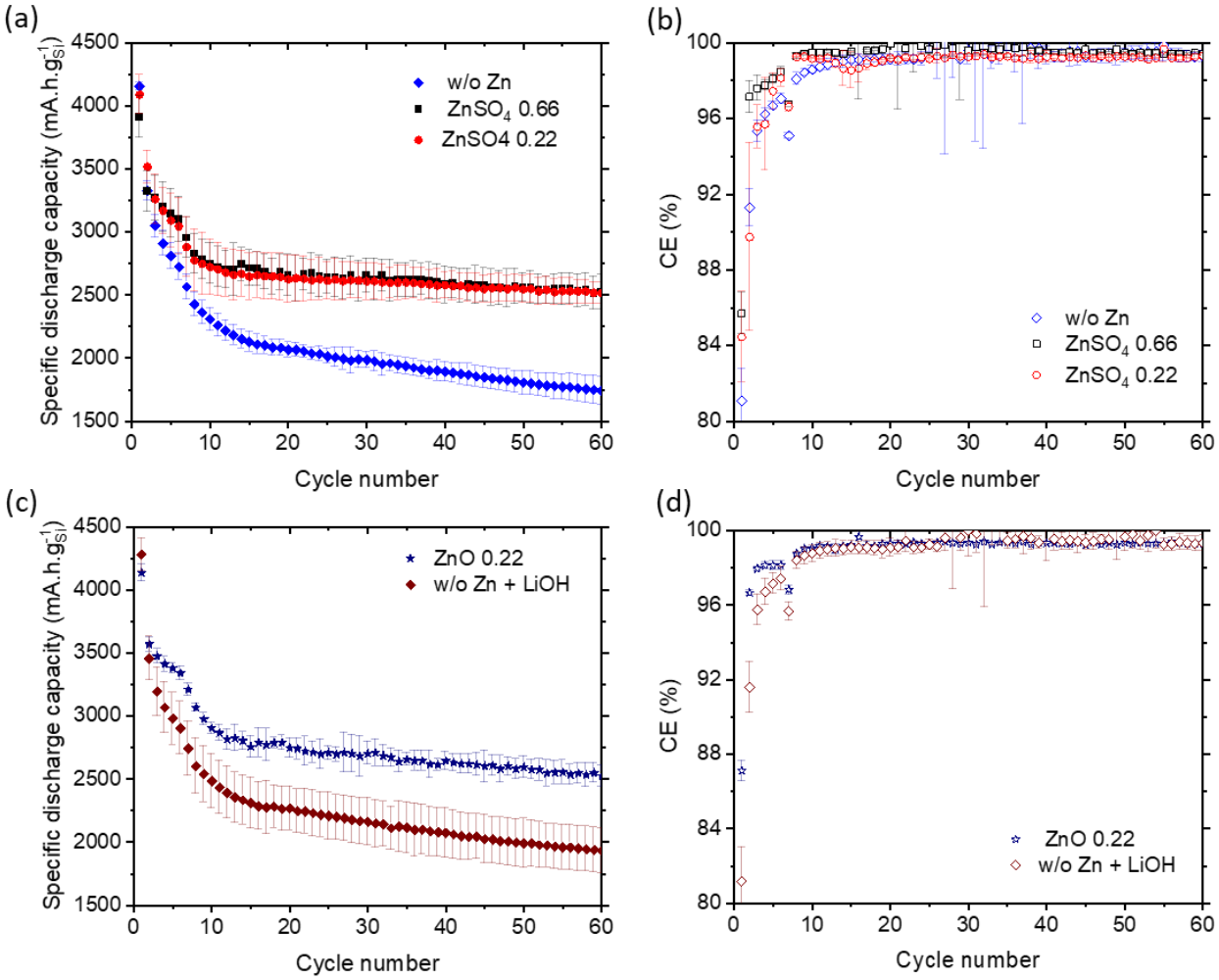

Figure 1. *Evolution with cycling of the specific discharge capacities and CE for 1.75 mg$_{Si}$.cm^{-2} electrodes: (a, b) Formulations based on ZnSO$_4$; (c, d) Formulations based on ZnO. The C rate was C/40 for the 1st cycle, C/20 for the next 5 cycles and C/10 for the subsequent cycles.*

Both formulations containing $ZnSO_4$ perform similarly and are clearly superior to the reference with a discharge capacity of about 2520 *vs.* 1740 mAh.g$_{Si}^{-1}$ at the 60th cycle. Moreover, the capacity loss rate is much more pronounced for the latter, which reaches approximately 9 *vs.* only 3 mAh.g$_{Si}^{-1}$ per cycle for electrodes containing $ZnSO_4$. This improvement is remarkable considering their high active mass loading of 1.75 mg$_{Si}$ cm^{-2}, which corresponds to a surface capacity of 6.3 mAh cm^{-2}, which is greater than the commercial graphite electrodes and even graphite with a little silicon added. A high Si mass loading means large mechanical strain

associated with the Si volume change within the coating and at the interface with the current collector, likely to accentuate the mechanical degradation (cracking and delamination) of the electrode and thus inducing its rapid capacity decay upon cycling. Therefore, most studies published in this field relate to low weight silicon-based electrodes, typically 1 or less than 1 mg cm^{-2}, which are not very representative of industrial needs, contrary to our work.

Figure 1b shows the coulombic efficiency (CE) of the three formulations at each cycle. For the first cycle, the CE are around 86, 85 and 81%, for the formulations corresponding to $ZnSO_4$ (0.66), $ZnSO_4$ (0.22) and no Zn, respectively. For the next 5 cycles (C/20 cycling), the $ZnSO_4$ (0.66) formulation presents a significantly better CE. Both reference and $ZnSO_4$ (0.22) formulation CE fluctuate and overlap. Finally, from about the 20^{th} cycle (cycling at C/10), the CE stabilizes at around 99.6, 99.2 and 99.4% for $ZnSO_4$ (0.66), $ZnSO_4$ (0.22) and no Zn, respectively. This corresponds to the period where the electrode capacity declines linearly with each cycle. Interestingly, the CE does not reflect the capacity loss per cycle. Overall, the Zn(II)-rich (Zn/RCO_2H = 0.66) electrodes have a higher CE at each cycle. Unfortunately, that does not translate into a better discharge capacity retention. In the end, the electrochemical performance stagnates (or even decreases) after a certain level of cross-linking is reached. This is in agreement with our previous findings on Cu-CMC-CA binder[15] as well as with the literature on covalently cross-linked binders.[6]

Figure 1c shows the specific discharge capacity per cycle (mean and standard deviation results from multiple cell tests, see **Table S1**), for the formulation containing ZnO (0.22) and the corresponding reference (prepared at a similar pH through the addition of LiOH). These electrodes have the same silicon loading as those in **Figure 1a**. Their initial capacity also exceeds the theoretical capacity by about 560 and 720 $mAh.g_{Si}^{-1}$ for the formulation containing

ZnO and corresponding reference, respectively. Again, by examining the dQ/dV curves (**Figures S2**), the capacity associated with the reduction of the binder components are shown to be negligible in line with the absence of significant reduction peaks associated with protons from carboxylic acids and Zn(II). Using again ^{7}Li NMR, the amount of Li in the SEI was evaluated (see **Table S2**); it reaches 363 mAh.g_{Si}^{-1} for the electrode containing ZnO (0.22), supporting the fact that the formation of the SEI is at the origin of this extra capacity. In fact, the main reduction peak(s) on the dQ/dV curves at 0.9-1.1 V (*vs.* Li^{+}/Li^{0}) seen for both formulations is associated with the reduction of FEC.[22,25,26] Interestingly, this phenomenon is more intense for formulations without Zn, which tends to confirm that the coordination with Zn increases the ability of the binder to act as an artificial passivation (SEI) layer. This result is in complete agreement with our previous STEM-EDX study on $ZnSO_4$-containing electrodes after one cycle, that evidenced that the surface of the silicon particles covered by the binder (including Zn) are exempt of standard inorganic SEI components (containing F and P).[19]

Like with $ZnSO_4$, the ZnO formulation capacity retention is higher than its reference formulation with a discharge capacity of about 2530 *vs.* 1930 mAh.g_{Si}^{-1} at the 60th cycle. The capacity loss by cycle is also higher for the latter, which reaches approximately 8 *vs.* 5.6 mAh.g_{Si}^{-1} for ZnO-containing electrodes. The CE for the formulation containing ZnO and its reference are shown in **Figure 1d**. For the first cycle, the CE are about 87 and 81%, respectively. The latter formulation's CE remains lower until the 20th cycle, at which time it stabilizes at approximately 99.5 *vs.* 99.3% for ZnO-containing electrodes.

In sum, we confirmed that the straightforward addition of a Zn(II) precursor (whatever its nature, see also **Figure S3b** for the electrochemical performance with addition of $Zn(NO_3)_2$) to an aqueous CMC-CA formulation leads to a significant improvement of the electrochemical

performance, notably to an improved CE and a better capacity retention. Consequently, Zn containing binders, inks, and electrodes were further studied with the aim of establishing relationships between their microscopic structures, macroscopic mechanical properties, and electrochemical performance.

Characterization in solution of binders and inks.

Figures 2a and **2b** show the viscosities as a function of the shear rate for the binder solutions $ZnSO_4$ (0.66), $ZnSO_4$ (0.22), and their reference, as well as the respective inks (*i.e.* containing also Si and graphene). The extensive rheological studies of NaCMC aqueous solutions by Lopez et al. [27–33] is at the basis of our results analysis. The degree of substitution (D.S.), which represents the average number of sodium carboxylate groups per monomer, is an important parameter that dictates the solubility of NaCMC in water. In fact, the cellulose backbone is hydrophobic, whereas the carboxylate/ic groups are hydrophilic. In our case, the D.S. is equal to 0.9 (from supplier data), which is enough to solubilize the polymer. However, because it is inferior to 1, a significant monomer fraction is unsubstituted,[27] which might recur in large polymer segments without interruption, as the substitution is not homogenous. With increasing polymer concentration, inter-chain polymer interactions develop and result in hydrophobic behavior, leading to increased viscosity and eventually gelation.[28] This is particularly true for our formulations, as the NaCMC concentration is 83 mM (*i.e.* 19.5 g/L, approximately 2 $_w$%) and the degree of polymerization reaches approximately 3000, such that our binder can be considered as a concentrated entangled NaCMC solution.[29] The addition of inorganic bases (here LiOH, NaOH or KOH) may help to solubilize the unsubstituted polymer blocks, reducing the hydrophobic behavior,[28,34] but it typically requires higher concentrations

than the ones used in the present study. For example, 7-10 $_w$% of NaOH is required to dissolve cellulose[34] and 0.5 M NaOH was found to be insufficient to totally remove hydrophobic interactions for NaCMC with a D.S. around 0.8.[30]

In a more general manner, the presence of salt has the effect of charge screening along the polymer chains. However, the distance up to which the polymer chain behave like a rigid rod,[27] *i.e.* the intrinsic persistence length, depends on the electrostatic contribution (among others).[29] While the electrostatic interactions are screened by salts,[28] the chain dimension evolves from rod-like to worm-like.[28,29] As such, the solution viscosity decreases as the chain flexibility increases. It is also reported to reduce the solvent quality exponent[35] without influencing its entanglement properties.[29,35] Even if divalent salts (here Zn(II) precursors) display increased ionic strength over monovalent ones, inducing a greater screening,[31] the electrostatic interaction are most likely already screened for our formulations. In fact, at our NaCMC concentration, the chains should be highly screened even in a salt free solution (*i.e.* not buffered), simply because of the presence of Na^+ associated with NaCMC.[32]

As shown in **Figure 2a**, the viscosity at 0.01 s^{-1} is significantly higher for the $ZnSO_4$ (0.22) formulation than for the Zn-free binder solution with around 300 *vs.* 60 Pa.s, respectively, both of which are higher than the 30 Pa.s of the Zn-rich binder ($ZnSO_4$ (0.66)). The increase in viscosity at low shear rate upon addition of Zn(II) could be due to electrostatic interaction (*i.e.* coordinative bridging) between the carboxylates groups and Zn(II) ions. At our given CMC concentration, the viscosity increase could reach up to an order of magnitude thanks to the interchain cross-linking.[33] Here, the value is lower, probably because a significant part of Zn(II) ions are solely coordinated to CA, rather than to CMC. The viscosity decrease upon further addition of Zn(II) (*i.e.* for $ZnSO_4$ (0.66)) relates to a different phenomenon. Sharratt et

al.[31] showed that upon addition of a higher amount of a metallic salt to a solution of NaCMC, a transition from a monophasic to a biphasic solution occurs. In the case of Zn(II), CMC forms aggregates with an estimated diameter of 26 nm. Interestingly, this behavior was only found for divalent cations specifically interacting with CMC, such as Ca(II), Zn(II) and Ba(II), but not Mg(II).[31] Based on the previously published data, at our given CMC concentration, slightly more than 40 mM of Zn(II) salt would be required for this transition (for a D.S. of approximately 1.3). In our study, we used a 2 to 6 times (Zn/RCO_2H = 0.22 and 0.66, respectively) higher concentration. For the latter, the binder solution is most likely in the biphasic state, with the polymer chain folding into aggregates with intra-chain Zn(II)-carboxylate interactions, leading to a lower viscosity. For the Zn-poor formulation ($ZnSO_4$ (0.22)), it is possible that the monophasic to biphasic boundary is not crossed, because a fraction of Zn(II) is interacting with CA instead of CMC. With increasing shear rate, the viscosity decreases due to chain alignment in the flow direction as well as disruption of inter-chain short contacts (due to hydrophobic interactions, coordination, and steric/entanglements). The higher ionic strength in the Zn-containing inks might then increase the CMC chains folding, which increases the attractive intra-chain interactions. This process might explain the fact that the Zn-free inks are more viscous than Zn-containing ones at high shear rate.

Figure 2b present the viscosity as a function of the shear rate for the binder containing ZnO (0.22) and its reference. In contrast to our finding with $ZnSO_4$, the viscosities of both formulations are almost identical. This is at a first sight surprising, but could be related to the pH of the solutions: at least from a thermodynamic viewpoint, cation-carboxylate complexes are stable in a given pH range but they can dissociate at pH higher than the pKa of the carboxylic/carboxylate couple.[36] For the given formulations, the pH of the binder solution

containing $ZnSO_4$ (*i.e.* 2.9) and ZnO (*i.e.* 4.3) are respectively, lower and higher than the pKa of NaCMC (≈ 3.4). Zn(II) might then interact to a lesser extent with the CMC carboxylate groups upon addition of ZnO than $ZnSO_4$, reducing the interchain cross-linking and therefore the viscosity. In these experimental conditions, *i.e.* with ZnO, most of the Zn(II) ions might then be more likely complexed by CA (in the form of molecular complexes), which presents higher second and third pKa_s (4.76 and 6.40). We further attempted to investigate the carboxylates in solution for the $ZnSO_4$ and ZnO (0.22) binders by Raman spectroscopy (λ = 514.53 nm, dispersive Raman spectrometer coupled to a confocal microscope; Renishaw Invia). Unfortunately, almost no signal was recovered most likely due to the light diffusion in the viscous and slightly opaque/turbid binder solutions. Therefore, no information was retrieved.

The different rheological behaviors of the binder observed here show a complex interplay between pH, the presence of both salts/molecules, and divalent cations. These parameters also govern the binder states at rest, as can be seen from the storage and loss modulus curves shown in **Figures S5a and S5b**. In fact, only the $ZnSO_4$ (0.22) binder behaves like a physical gel (G' > G'') and exhibits a small G" overshoot above 20% strain, proving that the binder is cross-linked, which is also in line with the viscosity results.

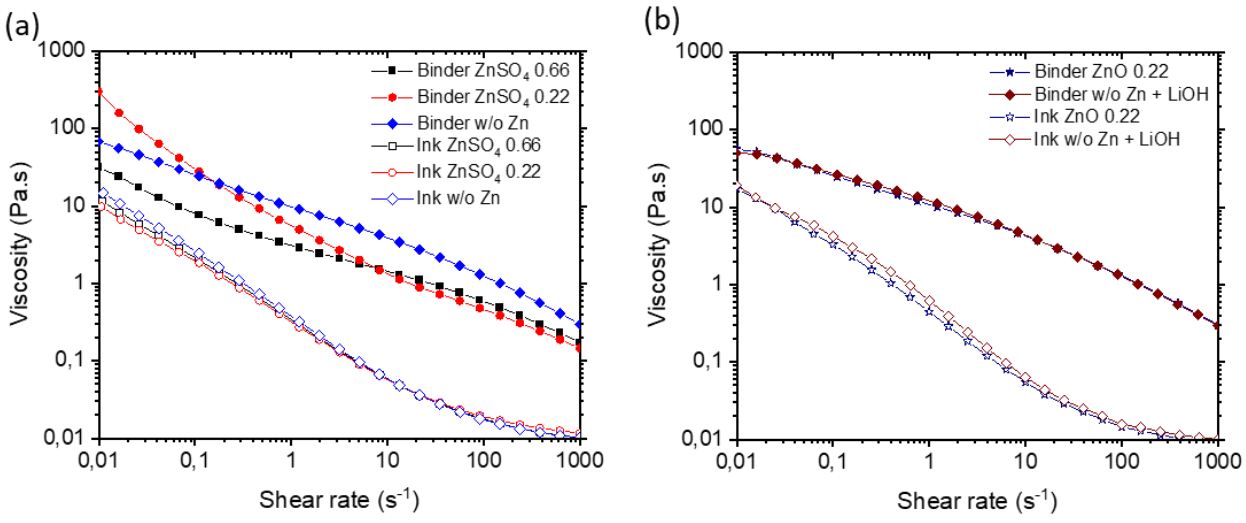

Figure 2*. Viscosity as a function of shear rate of binder solutions and respective inks: (a) Solutions based on $ZnSO_4$; (b) Solutions based on ZnO.*

The ink (binder solution with Si and graphene) viscosity was also studied (**Figures 2a** and **2b** for the inks containing $ZnSO_4$ and ZnO, respectively). All inks behave similarly, indicating that their viscosity seems insensitive to the binder composition. Hence, the solid fraction (especially of silicon and graphene) in the ink, which is the same for all formulations, seems to determine their rheology. During tape casting, the shear rate applied by the blade is equal to the tape casting speed divided by the blade gap. It is approximately 37 s^{-1}, for a 150 µm blade gap. The respective ink viscosity is 28 $mPa.s^{-1}$, which represents very little flow resistance. Nonetheless, at rest (equivalent to a low shear rate) the viscosity is enhanced, which is interesting for slurry stability during drying. For this latter step, the yield stress is a better indicator, as it is the necessary force to induce flow and hence represents the percolating network strength. It is usually extracted from the shear stress curves (**Figures S4**) by using for example a Herschel-Bulkley model fit. However, this method did not seem appropriate in our case, and the reader is referred to the SI and **Figure S4** for explanations. Therefore, the shear stress value at 0.01 s^{-1} was selected as the yield stress. Among the $ZnSO_4$-based inks, it is approximately equal to 0.16, 0.10 and 0.13 Pa for Zn-free, $ZnSO_4$ (0.22) and $ZnSO_4$ (0.66), respectively. For the ZnO-based inks, it is equal to 0.19 and 0.17 Pa for Zn-free and ZnO (0.22), respectively. Overall, the yield stress is of the same order of magnitude for all formulations and remains fairly low (but consistent with the solid fraction used here[20]). These values are such that segregation or settling could occur over time if the ink drying is too fast or too slow, respectively.[37]

Localized characterization in the solid state of binders and electrodes.

Figures 3 show the IR transmittance spectra of solid products obtained after drying the binder solutions at 100 °C (see the experimental section for details). For the $ZnSO_4$-containing binder ($ZnSO_4$ (0.22) and $ZnSO_4$ (0.66), **Figure 3a**), in order to prevent any overlap between the bands arising from the water (υ_{2b} bending mode of H_2O at approximately 1645 cm^{-1} [38]) and carboxylic/carboxylate groups, solutions were formulated with D_2O instead of H_2O. For every composition, three bands are visible in the range 1300-1800 cm^{-1}: a first one at 1700-1715 cm^{-1} associated to C=O vibrations of protonated carboxylic groups, and two other ones at 1570-1610 and 1370-1400 cm^{-1} attributed to asymmetric and symmetric carboxylate vibrations, respectively. They clearly indicate that each binder contains both non-bonded carboxylic groups and carboxylate groups likely in interaction with the cations. The ν_{asym} and ν_{sym} peaks of the carboxylates are particularly broad, likely because they contain multiple contributions. This is clearly visible for Zn/RCO_2H = 0.22 and 0.66 and for $Zn(NO_3)_2$ (0.22) in **Figure S3a**. This is expected considering that the binders contain several cations (Na^+, K^+, Zn^{2+}) and several types of carboxylic/ate groups arising both from CMC and CA. Their convolution causes this broadening and prevents any deep analysis for lack of resolution. Indeed, for simple compounds (*e.g.* model metal-carboxylates complexes), the difference $\Delta\upsilon_{asym}$-υ_{sym} can be used as a mean to propose a possible M-carboxylate coordination motif,[39,40] but such an approach cannot be applied here. However, when compared to the reference formulation, the addition of $ZnSO_4$ induces a significant shift towards higher wavenumber of both the υ_{asym} (23 and 29 cm^{-1} for $ZnSO_4$ (0.22) and $ZnSO_4$ (0.66), respectively) and υ_{sym} vibration bands (17 and 23 cm^{-1} for $ZnSO_4$ (0.22) and $ZnSO_4$ (0.66), respectively). These shifts are indicative of the different environments for the carboxylate groups, in agreement with the formation of Zn(II)-carboxylate coordination bonds.

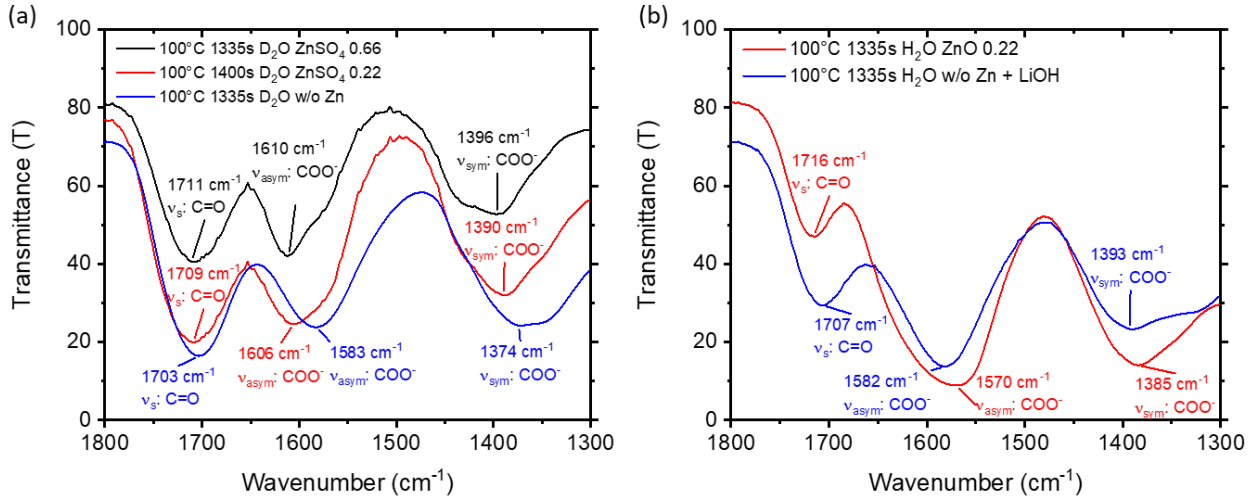

Figure 3. *IR spectra of dried binders: (a) Solutions based on $ZnSO_4$, which were prepared with deuterated water; (b) Solutions based on ZnO, which were prepared with ultra-pure water. The time stamp in each legend refers to the time at which the spectra was acquired, while the sample was still heated.*

The same experiment was conducted for binders prepared with ZnO (0.22) and their reference, this time using H_2O (see **Figure 3b**). No H_2O υ_{2b} vibration band was clearly resolved, but the presence of the $2\upsilon_{2b}$ and υ_1 large bands above 3000 cm^{-1} (not shown) clearly indicates the presence of water in the samples.[38] Both the υ_{asym} and υ_{sym} were shifted upon addition of ZnO when compared to the Zn-free reference (-12 and -7 cm^{-1}, respectively), again in agreement with the presence of different local environments for the carboxylates and likely the formation of Zn(II)-carboxylate bonds. Nevertheless, whereas these bands were upshifted with $ZnSO_4$, they are downshifted with ZnO. Furthermore, the values of $\Delta\upsilon_{asym}$-υ_{sym} are also different (191 and 186 cm^{-1} for Zn-free and ZnO (0.22), respectively). This suggests that the coordination modes might be different between both $ZnSO_4$ (0.22) and ZnO (0.22) formulations. This could arise either because different coordination motifs are favored depending on the pH, as suggested by rheological measurements (more Zn(II)-CA complexes and less Zn(II)-CMC ones with ZnO), or because the counter ion is different (SO_4^{2-} might still be interacting with Zn(II)). Alternatively,

this difference could come from the variation of the number of protons surrounding the carboxylates with the pH.

It was not possible to carry out the same experiment for the binders in solution as only the signal of the solvent would be visible. Nonetheless, similar features were observed for the partially dried solutions (heated at 60°C, **Figure S6**), suggesting that the Zn-carboxylate coordination bonds already exist in the hydrated binder, hence supporting our interpretations of the rheological results.

In sum, these IR analyses suggest the presence of carboxylate-Zn(II) bonds in the solid, but no definitive information on the nature of the coordination motif and the origin of the carboxylate groups (CMC and/or CA) was obtained. In an attempt to gain additional information, ^{17}O solid state NMR experiments were carried out. ^{17}O is a spin-5/2 quadrupolar nucleus having a low natural abundance (0.04%).[41] ^{17}O NMR signals of carboxyl and carboxylate groups can spread over a wide chemical shift range and present large quadrupolar coupling constants. The Zn-free, $ZnSO_4$ (0.22), and the ZnO (0.22) binders were prepared using ≈ 40% ^{17}O enriched CA (enriched on carboxylic functions by adapting a previously published procedure).[42] Thus, only the signal of carboxylic/ate groups from the CA molecules is expected to be visible on the ^{17}O NMR spectra (and not the CMC ones). The corresponding spectra are shown in **Figure S7** together with the ones of the ^{17}O-enriched CA and the Zn-citrate coordination polymer $Zn_3(CA)_2(H_2O)_2$ (prepared following a procedure published elsewhere[43]). For pristine CA, signals with sharp and well-defined features are visible in the region characteristic of carboxylic acid groups, as is expected for a crystalline starting material. The line shapes reflect the effects of the second-order quadrupolar interaction, as ^{17}O is a spin 5/2 isotope. For the reference Zn-free electrode, a ^{17}O NMR signal is also seen, indicating the presence of labeled CA, as expected.

However, in contrast to crystallized CA, this signal exhibits a clear asymmetry due to an electric field gradient distribution (which is associated with the quadrupolar interaction). This suggests that CA is present only in a disordered form in the binder, which may be indicative of its homogenous mixing with CMC. Upon addition of Zn(II) (whatever the precursor), again a signal characteristic of disordered carboxylate environments is detected. Nevertheless, while significant differences in ^{17}O signatures of CA could have been expected upon complexation of Zn(II) (as shown in **Figure S7a**, when comparing the ^{17}O NMR data of crystalline CA and $Zn_3(CA)_2(H_2O)_2$), the variations between the ^{17}O signatures of the binders (whether containing Zn(II) or not) were actually less pronounced, showing in all cases broad asymmetric line shapes with a maximum peak position at approximately 180 ppm at 11.7 T. Further analyses in another magnetic field would be needed to pinpoint the changes in chemical shift and quadrupolar parameters upon complexation and try to extract information regarding the nature of the CA cation-carboxylate interactions. Nevertheless, and importantly, these preliminary ^{17}O NMR experiments tend to suggest a homogeneous distribution of the CA inside the binder (with or without addition of Zn(II)), leading to a distribution in local carboxylic/carboxylate environments.

Electrode preparation requires intensive mixing and drying steps which could have an impact on the materials distribution. Therefore, binder coordination was also evaluated in the electrode conditions by ^{1}H-^{13}C CP-MAS-NMR. The analysis was performed on binders mixed with silicon (in the same quantities as for electrodes), but without graphene to avoid signal masking. Four formulations were considered: the formulations containing $ZnSO_4$ (0.22) and ZnO (0.22), and their respective references. The corresponding spectra are presented in **Figure S8a**. For each composition, all the signals characteristic of the CA and CMC were detected as

expected. The signals centered at approximately 170-180 ppm are of particular interest as they correspond to the carboxylic/ate groups and thus are a priori sensitive to the formation of coordination bonds.[44] As a matter of fact, for all electrodes, a broad and unresolved signal centered at 180 ppm was detected which showed variations in peak maximum position and line width depending on the binder composition. This suggests changes in protonation state and/or cations bonded to the carboxylic/carboxylate functions between the different electrodes. Indeed, the ^{13}C NMR analysis of reference molecular compounds (NaCMC, CA, Na_3CA and $Zn_3(CA)_2$, **Figure S8d**) indicates that the signal shift related to the carboxylates can reach 3-8 ppm upon complexation of metal cations. Here, the ^{13}C peak maxima of the more acidic electrode formulations were on average at lower chemical shifts compared to those of the more basic formulations (see discussion related to **Figure S8** in the SI). A more systematic investigations on the Zn(II) quantity influence and the degree of protonation of carboxylic/carboxylate groups in these systems would be needed to go further in the interpretation of these ^{13}C NMR results, though this is beyond the scope of the present work.

None of the spectroscopic techniques described above lead to a clear conclusion regarding the relative involvement of CA and CMC in the coordination network. One could argue that CA, having 3 carboxylic/ate groups, should interact more strongly with Zn(II) than CMC, and hence CA-Zn bonds are more favorably formed than CMC-Zn bonds. The relative amount of CA-Zn and CMC-Zn bonds might also vary between the different formulations, as it seems to be multifactorial (pH, Zn(II) precursor, concentration). Rheological studies showed that Zn(II) cations, which are preferentially interacting with carboxylate groups,[31,33] do not always lead to CMC inter-chains crosslinking in solution (through coordination bonds). Therefore, this raises questions on the possible predominance of one type of coordination bond *vs.* the other and

its relationship with the electrochemical performance enhancements. We attempted to answer these questions by replacing CA in the binder solution by piperazine-N,N′-*bis*(3-propanesulfonic acid) (PIPPS), which has a similar first pKa_1 (≈ 3.7 *vs.* 3.1 for CA) but is less complexing (it is indeed commonly used to prepare non-complexing buffer in biochemistry). Electrodes were prepared both with and without $ZnSO_4$. The correspondings specific discharge capacity and coulombic efficiency are shown in **Figures S9a** and **S9b**, respectively. In the absence of Zn(II), the specific capacity dropped down within very few cycles (< 500 mAh g^{-1} after 10 cycles). In the presence of Zn(II), the capacity retention is far better, with a specific capacity still above 1000 mAh g^{-1} after 50 cycles. As Zn(II) should predominantly interact with CMC in the latter formulation, this experiment is evidence of the direct relationship between the formation of Zn-CMC bonds (and therefore probably of extended coordination network) and the capacity retention improvement. However, the capacity is still lower than the one observed for the formulation containing CA instead of CMC (see **Figures 1a** and **1b**). This indicates that CA also has a pivotal role, for example acting as a co-ligand in the coordination network and/or as an artificial passivation layer on Si, as was already reported by Lucht et al.[45,46]

Note that it was not possible to characterize the binder in cycled electrodes because the organic products of electrolyte degradation mask the binder, which is otherwise found in small quantities and hidden at the interfaces. However, the fact that after 50 cycles the difference in capacity between the zinc-based binder and its zinc-free reference electrodes continues to increase suggests that the Zn(II)-poly(carboxylates) reticulation is maintained upon extended cycling.

Characterization of the electrode mechanical properties at the macro and microscopic scales.

The electrode mechanical properties were studied in order to evaluate the benefit associated with the presence of coordinated binder. First, scratch tests allow the evaluation of both cohesion and adhesion strengths (see SI and **Figure S10** for details). The critical scratch load as a function of the electrode silicon loading for every formulation is shown in **Figure 4.** It corresponds to the load upon which the current collector is visible at the bottom of the scratch (see an example in **Figure S10**). As expected, whatever the formulation, the critical load increases with the silicon loading, hence the quantity of matter plowed.[47]

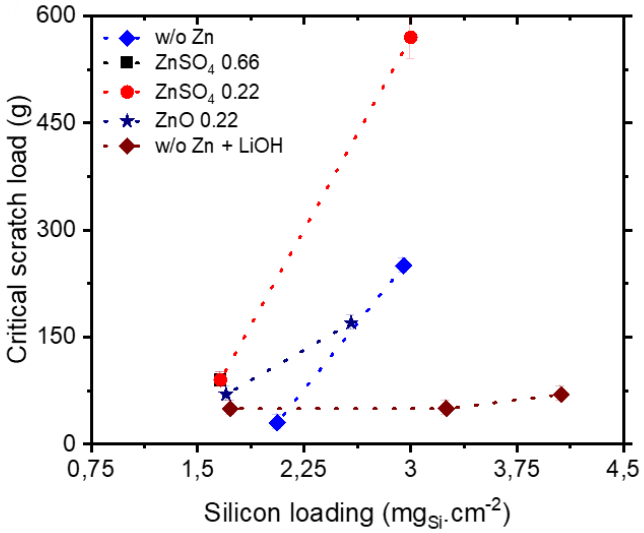

Figure 4. *Critical scratch load as a function of the silicon loading of the different binder electrode coatings.*

The trend between coordinated binders and their respective references is clear. Whatever the Zn(II) precursor, all coordinated binders have higher critical scratch load than their non-reticulated reference over the whole loading range tested. For example, at approximately 1.7 $mg_{Si}.cm^{-2}$ (corresponding to the electrodes used for the electrochemical studies), the critical load

is 40% higher for the ZnO (0.22) containing coating than for its reference. Thus, binder Zn-carboxylate coordination enhances both adhesion and cohesion strengths.

The effect of the amount of cation was also evaluated with $ZnSO_4$. Again, for a loading corresponding to the electrodes used in the present study, both the Zn(II)-poor ($ZnSO_4$ (0.22)) and Zn(II)-rich ($ZnSO_4$ (0.66)) electrodes present an identical critical load. This is in agreement with the absence of major differences in their electrochemical behavior (see **Figure 1**). In fact, for binders cross-linked through covalent bonds, an excess of the reticulation degree can produce an opposite effect on the mechanical properties, decreasing tensile strength as well as elasticity.[6]

If one compares the Zn precursors (at $Zn/RCO_2H = 0.22$) at a given silicon loading, the electrodes formulated with ZnO present lower critical loads than the ones formulated with $ZnSO_4$. Three phenomena can explain this lower adhesion/cohesion, and all rely on the pH of the ink (2.9 and 4.3 for $ZnSO_4$ and ZnO, respectively). First, a lower level of coordination cross-linking of the CMC chains can be expected (see the discussion above). Second, the binder is bonded to the silicon surface through either weak hydrogen bonds, or strong silyl-ester covalent bonds (formed upon drying). The former happens between carboxylic acid and silanol and the latter comes from their condensation reaction which occurs upon drying the electrode.[15,48,49] The formation of silyl-ester bonds is favored at acidic pH.[50] Hence, a lower ratio of strong silyl-ester bonds to weak hydrogen bonds (if any) is expected in the formulation based of ZnO than $ZnSO_4$. Third, the copper current collector corrosion is also favored at $pH \approx 3$.[15,21] This induces the formation of strong Cu(II)-carboxylates bonds between the binder and the current collector and throughout the whole electrode.[14] At $pH \approx 5$, Roland et al[51] did not found any dent in the copper. There is only a scarce presence of copper (as Cu-carboxylate) through the

electrode thickness, which anyway, reveal a slight current collector corrosion. Overall, the three mechanisms explain the lower adhesion and cohesion of the formulation containing ZnO than the one containing $ZnSO_4$.

Nano-indentation experiments were further used to determine the electrode hardness and elastic modulus, both in the dry state and wetted with propylene carbonate solvent (the latter is easier to handle than the LP30 + 10 $_w$% FEC electrolyte). Studies were also conducted by micro-indentation, which gave similar results, although impacted by the current collector mechanical properties and the reduced porosity (see SI and **Table S4** for details). **Table 3** presents the hardness and elastic modulus obtained for the electrodes containing $ZnSO_4$ (0.22) and the corresponding reference. Typical hardness and elastic modulus depth profile are available in **Figure S11**. Again, both electrodes have similar active mass loadings, which are also relevant compared to the 1.75 ± 0.1 $mg_{Si}.cm^{-2}$ electrodes selected for electrochemistry. However, their porosities are quite different, with 56.6 *vs.* 66.2% for the electrode with and without $ZnSO_4$, respectively. Specifically, these values are slightly lower (for the former) and higher (for the latter) than their cycled counter parts (see **Table S1**), though in the same range as the ones found for the other electrodes. It is difficult to quantify the impact of the porosity on the mechanical properties. Qualitatively, both the compressive elastic modulus and the hardness are expected to decrease with porosity. However, the relationship is not linear, and two stages are succeeding. In the first, the porosity is high, and the indenter will densify the electrode by deforming the matrix. In the second, the porosity is low, and the electrode is already compact, thus the indenter will deform the silicon and graphene particles (because they represent a higher volume fraction than the binder). At this stage, hardness and elastic modulus dependence on porosity is at its highest.[52] In our case, the electrodes are mostly porous, so the impact of their porosity

difference should be minimal. Looking at the results, in the dry state, the hardness and elastic modulus of the electrode containing $ZnSO_4$ are about 2 and 1.5 times higher than the reference electrode ones, respectively. This confirms that the binder Zn-carboxylate reticulation significantly enhances the coating cohesion strength. It is interesting to see that Cuauhtémoc et al.[14] found a similar magnitude of improvement with a formulation equivalent to Cu-CMC-CA, although using micro-indentation, whose differences with nano-indentation are explained in the discussion associated to **Table S4**.

Table 2. *Mechanical properties assessed by nano-indentation of a $ZnSO_4$ (0.22) and its reference electrodes, in both the dry state and soaked in propylene carbonate.*

Salt	*Coord. Ratio*	*Film condition*	*Active mass loading ($mg_{Si}.cm^{-2}$)*	*Porosity ($_v$%)*	*Hardness (Mpa)*	*Elastic modulus (Gpa)*
w/o Zn	0	dry	1.93	66.2	25 – 45	1.5 – 2.5
w/o Zn	0	electrolyte	1.93	66.2	15 – 20	1 – 1.5
$ZnSO_4$	0.22	dry	1.86	56.6	50 – 60	3 – 4.5
$ZnSO_4$	0.22	electrolyte	1.86	56.6	50 – 65	3 – 4.5

When soaked in propylene carbonate (to mimic the electrolyte), only the reference electrode showed reduced mechanical performance. Wang et al. already reported this behavior for silicon electrodes formulated with NaCMC (and other binders).[52] It is known that NaCMC can uptake around 10 to 20 $_w$% of carbonate based electrolyte.[53,54] Such an uptake should induce a rather small swelling,[55] but it appears sufficient to reduce the electrode mechanical properties. Remarkably, for the electrode containing $ZnSO_4$, the hardness and elastic modulus remain nearly unchanged after electrolyte soaking. They are approximately 3 times higher than the standard electrode in this state. The fact that the mechanical properties are nearly insensitive to the electrolyte means that, upon binder reticulation, its electrolyte uptake and successive

swelling decrease. This effect could arise from the immobilization of polymer segments, which is expected for chemically cross-linked binders.[6] Such a reduced uptake was already reported by few groups for Ca(II)-Alg reticulated binders,[9,13] although opposite behaviors were also measured.[10] Eventually, the binder reticulation through coordination bonds not only improves the mechanical property of the pristine electrode in the dry state, but also preserves them in presence of a carbonate solvent. Then, the question arises: how is this improvement going to impact the electrodes mechanical properties during lithiation/delithiation? To answer this question, *operando* dilatometry experiments were carried out.

Characterization of the electrode mechanical properties from *operando* dilatometry

Figures 5a and **5b** show the thickness variation of a $ZnSO_4$ (0.22) electrode and its Zn-free reference, respectively. Both electrodes were cycled under galvanostatic conditions at a C/40 rate. The first one was duplicated in order to evaluate the experiment reproducibility (see **Figure S12b**). Their silicon loading is around 2 $mg_{Si}.cm^{-2}$, *i.e.* similar to the one used for electrochemical cycling. A 120 µm thick current collector was used to avoid any bending of the electrodes upon the dilatometry measurements, as was observed with the standard 20 µm thick one (not shown). This bending likely comes from the lower pressure applied on the working electrode inside the dilatometry electrochemical cell compared to the standard Swagelok cells (1.3[56] *vs.* 15.9 N, *i.e.* approximately 17 *vs.* 202 kPa). This lower pressure is also known to reduce the overall electrochemical performance obtained with the dilatometry cell.[56,57] The discharge capacity was limited to 1200 $mAh.g_{Si}^{-1}$ since it was not possible to cycle the Zn-free reference electrode at full capacity. It was only possible to do so for the electrode containing $ZnSO_4$ (see **Figure S12a**). Nonetheless, at full or limited capacity, the electrochemical

performance of both formulations was rather poor in dilatometric cells compared to standard Swagelok cells (**Table S1**). Therefore, only the first cycle is discussed.

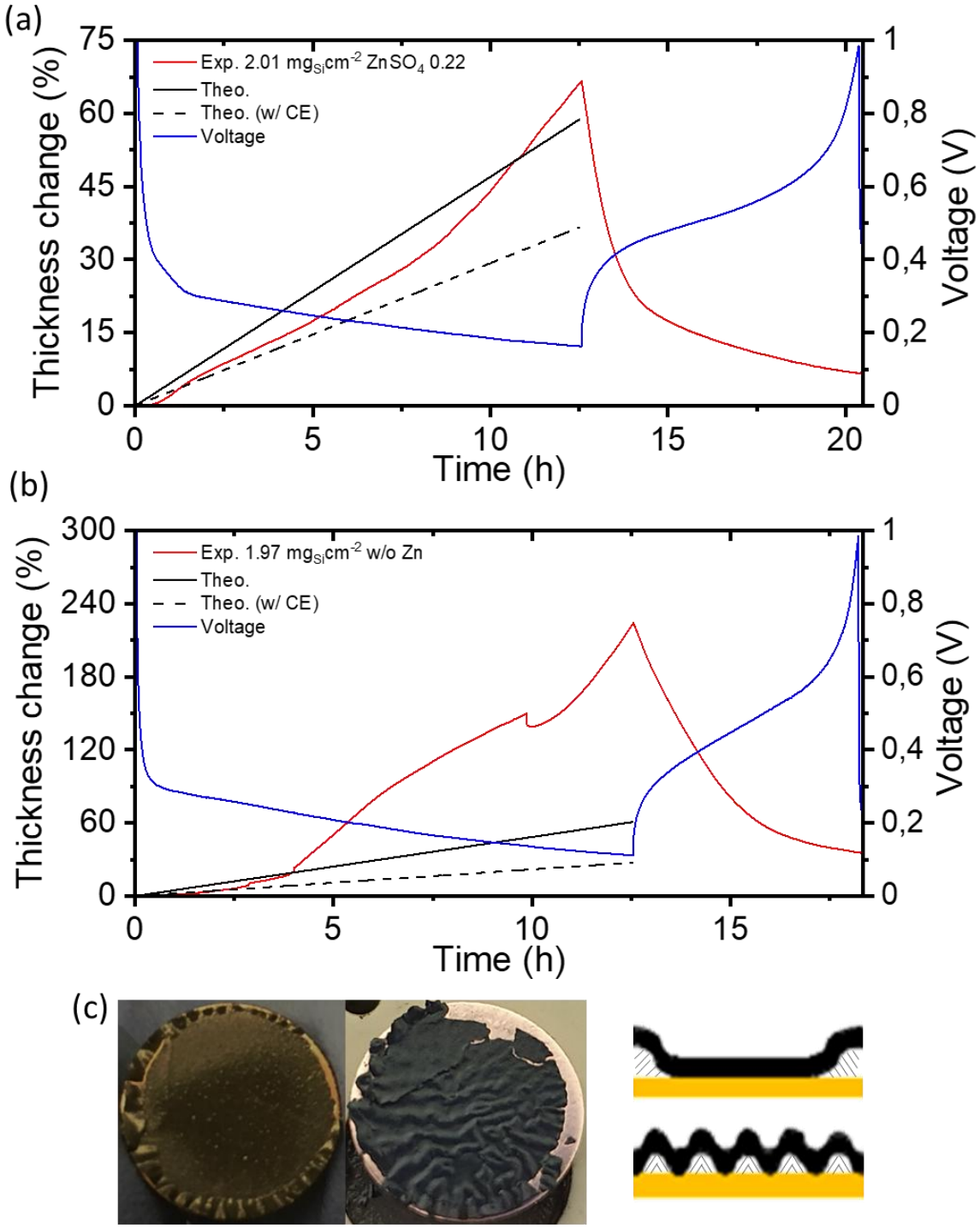

Figure 5*. (a,b) Experimental and theoretical thickness variation and voltage as a function of time (with a discharge capacity limited at 1200 mAh.g_{Si}^{-1}): (a) Electrode containing $ZnSO_4$ (0.22); (b) Zn-free reference electrode. The theoretical curves were calculated from Eq. (2)*

(black solid line) and Eq. (3) (black dash line); (c) Postmortem electrode pictures (left: containing $ZnSO_4$, right: without Zn(II)) and schematic representation of their buckling (top: containing $ZnSO_4$, bottom: Zn-free), not to scale.

The results are clear: while the thickness expansion for the reference electrode reaches 224% at the end of the first discharge at 1200 mAh g^{-1}, it is only 67% for the electrode containing $ZnSO_4$. This confirms the great ability of the Zn cross-linked CMC/CA binder to limit the lithiation-induced volume expansion of the composite electrode.

The thickness is a 1D parameter whereas volume is a 3D parameter. However, the electrode expansion/contraction only occurs in the out-of-plane direction since the in-plane expansion is prevented by the fixed dimensions of the Cu substrate. It can thus be assumed that the measured variation of the electrode thickness is equivalent to its volume variation. Considering that the volume increase arises exclusively from the expansion of Si upon lithiation, it is possible to compare the theoretical and experimental volume (thickness) expansion using the following equation [56]:

$$\Delta V_{el} = \omega_{Si} \frac{\rho_{app}}{\rho_{Si}} \frac{\Delta V_{Si}}{(1-\varepsilon_0)} = \varepsilon_{Si} \frac{\Delta V_{Si}}{(1-\varepsilon_0)} \quad (1)$$

where ΔV_{el} stands for the electrode volume expansion ($_v$%); ω_{Si} is the silicon mass fraction in the electrode; ρ_{exp} is the apparent electrode density at the pristine state; ρ_{Si} is the true silicon density (2.33 $g.cm^{-3}$); ΔV_{Si} is the intrinsic volume expansion of the $Li_{3.75}Si$ phase and is equal to 280%,[58]; ε_0 and ε_{Si} are the pore and silicon volume fraction, respectively. The reader is referred to **Table S5** for the parameter values of the different electrodes. By taking the term (1-ε_0), we consider that that the volume expansion of Si is not buffered by the electrode porosity (*i.e*. the pore volume expand by the same factor that the Si particles).[59]

Equation (1) was modified to make it discharge (lithiation) time-dependent:

$$\Delta V_{el} = \omega_{Si} \frac{\rho_{app}}{\rho_{Si}} \frac{\Delta V_{Si}}{(1-\varepsilon_0)} \frac{\Delta t}{t} \quad (2)$$

where Δt stands for the experimental discharge time (h); t is the corresponding C-rate time for a complete discharge and is equal to 40 h in the present case as the C-rate is C/40.

The discharge capacity does not solely come from the silicon lithiation, but also from the electrolyte electroreduction (*i.e.* SEI formation). Hence, assuming as a first approximation that the irreversible capacity accounts solely for the SEI formation and this one does not induce any volume expansion, the theoretical thickness variation is corrected according to the following equation:

$$\Delta V_{el} = \omega_{Si} \frac{\rho_{app}}{\rho_{Si}} \frac{\Delta V_{Si}}{(1-\varepsilon_0)} \frac{\Delta t}{t} \, CE \quad (3)$$

where CE is the coulombic efficiency (expressed as a fraction). Note that the electrode mechanical degradation inducing electrical disconnection of some Si particles will also be reflected in the CE. As such, the theoretical volume expansion calculated from Eq. (3) can be seen as a lower limit.

For the electrode containing $ZnSO_4$ **(Figure 5a)**, the experimental thickness expansion is rather in accordance with the theoretical one, at least regarding the maximum expansion calculated from Eq. (2). This is also true for its duplicate shown in **Figure S12b**. On the other hand, when the electrode is cycled at full capacity (**Figure S12a**), its maximum expansion is much higher than expected from the theoretical curves (270% *vs.* 120-180%). This suggests that some changes occur in the electrode architecture, which are not considered in the theoretical calculation. Moreover, the thickness does not increase linearly with the discharge time. This point will be discussed later.

For the Zn-free reference electrode (**Figure 5b**), the thickness variation is far higher than expected from its theoretical curve and compared to the Zn(II) formulation. This may be due to

the electrode buckling, as shown on the postmortem picture of the electrode (see right image in **Figure 5c**). Note that for the $ZnSO_4$ electrode, buckling is also observed but only on the electrode circumference (see left image in **Figure 5c)**. Thus, its impact on the dilatometry response must be much less important. The thickness drop observed at around 10 h of discharge (equivalent to ~960 mAh g^{-1}_{Si}) most likely comes from the electrode structure collapse. Since the electrode without Zn(II) failed massively, it is difficult to compare in details the thickness variation for both formulations. However, this is additional proof that reference electrodes are mechanically weak compared to the reticulated ones. Nevertheless, it is interesting to investigate the failure mechanism.

Buckling of a coating is caused by a high compressive growth stress in combination with insufficient coating adhesion.[60,61] Therefore, the electrode buckling must occurred during lithiation in dilatometric cell. This is at the opposite of crack formation which happen upon delithiation.[60,61] Interestingly, electrodes used in dilatometry suffered of buckling and most likely of cracking, whereas only the latter occurred for electrodes cycled in Swagelok cells. This means that the pressure applied on the Si electrode upon cycling (12 times lower in dilatometric cell than in Swagelok cell as previously stated) has a major impact on its mechanical behavior and thus on its electrochemical performance. Buckling will not be discussed extensively as it is not the standard mechanical failure mechanism of electrodes, but details can be found in ref. [60]. Nonetheless, applying the one dimensional blister theory, the critical stress σ_c required for the film to buckle can be calculated.[60,61] Namely, the following proportional relationship holds:

$$\sigma_c \propto E(h/b)^2 \quad (4)$$

where E is the film elastic modulus (GPa); h is the electrode coating thickness (µm), and b is the half of the blister delaminated width (µm). The blister dimension b was measured on **Figure 5c** and is equal to 278 ± 22 and 271 ± 22 µm (on an average of 6 measurements), for the Zn-free and $ZnSO_4$ (0.22) electrode, respectively. Wet E values presented in **Table 2** were used together with the film thickness of 27.75 and 36.5 µm for the Zn-free and $ZnSO_4$ (0.22) electrode, respectively. The critical stress is approximately 6 times higher for the Zn(II) containing electrode, confirming again its superior mechanical properties. Equation (4) holds if $h \ll b$, which is reasonable in our case. Fully applying the critical stress formula[60,61] yields a value of 11 and 62 MPa for the Zn-free and $ZnSO_4$ (0.22) electrode, respectively. Thus, tens of MPa should be a lower limit estimation of the developed stress in our electrodes.

Silicon volume expansion follows the Vegard's law[62] such that it increases linearly with the alloying lithium content. Thus, one can expect the volume expansion of electrode to be linear with the discharge time as illustrated from the theoretical expansion curves shown **in Fig. 5 and S12**. However, none of the electrodes follows this trend. Several factors might explain this behavior:

- Although the main part of the lithium incorporated in the electrode part alloys with silicon, a significant fraction is involved in the SEI formation and in the graphene lithiation. This affects the kinetics of the electrode expansion, which depends on the amount of lithium reacting with silicon/graphene/SEI, all of them having different expansion coefficients. It also means that the electrode expansion kinetics might evolve with time (with periods of either acceleration or deceleration). For instance, as seen in **Figure 5a-b**, no thickness change is observed during the first ~40 min of discharge, *i.e.* at a potential higher than ~0.4 V, where SEI formation mainly occurs and not Si lithiation.

- Deformation (elastic or plastic, rupture) of the electrode constitutive elements (silicon, graphene, binder and SEI) is also expected.

- The electrode porosity and its evolution with cycling can impact on the electrode thickness variation.[56] Actually, the volumetric expansion of the $SiLi_x$ particles can be partially buffered by the electrode porosity, especially at low discharge capacities, which is not considered for the theoretical thickness expansion curve. On the other hand, as seen in **Figure 5a**, from about 8.5 h of discharge (equivalent to ~820 mAh g^{-1}_{Si}), a significant increase of the expansion rate (curve slope) is observed, which may indicate that the electrode porosity becomes ineffective in accommodating the volume expansion of the $SiLi_x$ particles. This can be due to their larger size in comparison with the electrode pore size so they impinge on each other.[63] This could then induce a rearrangement of the position of the $SiLi_x$ particles in the vertical direction, accentuating the electrode thickness expansion.[56] This rearrangement is larger when the electrode is cycled at full capacity, resulting in an expansion higher than expected from the theoretical curve (**Figure S11a**).

Upon delithiation, electrodes contract, but their contraction behavior is also non-linear. The factors mentioned for the lithiation hold true for the delithiation (including the SEI, which is also electrochemically evolving during delithiation[64]).

Focusing exclusively on the electrodes containing $ZnSO_4$, an irreversible thickness variation can be observed at the end of the delithiation. This behavior has been systematically observed in *operando* dilatometry[56,57,63,65–68] and is usually attributed to an incomplete silicon delithiation because of the electrical disconnection of some Si particles and/or an irreversible plastic deformation of the electrode.[56,57,65] However, it is very difficult to evaluate the relative significance of both mechanisms. Note that for the full-capacity cycled

electrode, a higher irreversible expansion is observed at the end of the first charge compared to the electrode cycled at 1200 mAh g^{-1} (67% *vs*. 7%), which means that, as expected, irreversible changes in the electrode architecture is accentuated with the increasing lithiation level (thickness expansion) of the electrode.

In sum, the electrodes containing Zn(II) present improved mechanical properties compared to their reference counterparts. This translates into enhanced adhesion and cohesion of the electrode coating, higher hardness and elastic modulus both in the dry state and when soaked in carbonates, and reduced expansion upon electrochemical cycling. This is very likely related to the formation of a reticulated coordination network. However, these coordination compounds also affect the SEI formation. Through a deep STEM-EDX study on similar electrodes prepared with $ZnSO_4$, we recently showed that the coordination compounds (comprising Zn, alkaline ions and the organic carboxylates) cover a significant Si particles fraction in the pristine state. After one electrochemical cycle and degradation of the LP30 + 10 $_w$% FEC electrolyte, elements participating to the SEI (particularly the inorganic F and P elements) are not found in these regions, suggesting that the coordination binder also act as an artificial SEI.[19] Similar STEM-EDX analyses were carried out on the electrode prepared with ZnO and lead to the same conclusion. As shown **Figure S13** in the pristine electrode, all elements involved in the coordination binder phase (Zn, Na, O, C) are well dispersed. After one cycle (**Figure S14**), the coordination binder elements constitutive are still present on all Si particles, but the richer area contain very little SEI characteristic elements, while the poorer area contain a larger amount of them (*e.g.* see the central part of the Si particle located in the image bottom part).

CONCLUSIONS

The straightforward addition of Zn(II) precursors to a well-established formulation of Si electrodes leads to a significant improvement of their electrochemical performance, notably the capacity retention. Spectroscopic investigations are in line with the formation of Zn-carboxylate coordination bonds, although the complexity of the formulations (comprising different cations: Zn, Na, K and complexing molecules: CMC, CA) prevents a precise description of the coordination motifs at play. Nevertheless, a controlled electrochemical study showed that each component (CA, CMC, Zn) is essential to reach a decent cyclability, suggesting the formation of complex, likely reticulated coordination compounds. Such coordination bonds profoundly impact the electrode mechanical properties in terms of adhesion to the current collector, cohesion, hardness, and elasticity, and ultimately lead to a reduced expansion of the electrodes during electrochemical cycling and improved toughness. Eventually, the beneficial effect of the coordination compounds on the electrochemical performance likely arises both from the electrodes mechanical strengthening and the formation of an artificial SEI at the surface of the Si particles. Considering the versatility offered by coordination chemistry, there is likely plenty of room to modulate the formulations composition and optimize the electrochemical performance. One issue will probably be to achieve a proper description of the resulting coordination network, both in the pristine state and upon cycling. The identification of simpler model formulations will help to address this issue. Eventually, the combination of such optimized binders with state-of-the-art micro/nano-structured silicon, as well as their integration within full-cells, are the logical next steps to confirm their practical interest for the enhancement of the performance of Li-ion batteries.

EXPERIMENTAL SECTION

Material preparation

Binder solutions

First, a pH 3 buffer solution (0.171 M of citric acid + 0.084 M of KOH/NaOH) was prepared by dissolving citric acid (99%; Sigma-Aldrich) and KOH or NaOH salt (> 98%; Sigma-Aldrich) in ultra-pure water. Then, 5 mL of buffer plus the volume of ultra-pure water needed to reach 8.2 mL of solution was used to dissolve 160 mg of NaCMC (Mw ≈ 700 000 $g.mol^{-1}$, D.S. 0.9; Sigma-Aldrich). The as-obtained solution was the reference binder (Zn/RCO_2H = 0). Finally, upon NaCMC complete and homogeneous dissolution, the Zn(II) precursor was added all at once, and left until homogenization. For the reference containing LiOH, $LiOH•H_2O$ (≥ 98%; Sigma-Aldrich) was also added all at once. For every step, solutions were magnetically stirred at room temperature. The water coming from the Zn(II) salts was taken into account to reach the final volume of binder solution (8.2 mL), whereas the approximately 15 $_w$% ad/absorbed water in NaCMC was not taken into account.

For this study, different precursors of Zn(II) were used: $ZnSO_4•7H_2O$ (Pure cryst.; Alfa Aesar), (99.99%; Alfa Aesar), ZnO (99.99%; Alfa Aesar) and $Zn(NO_3)_2•6H_2O$ (98%; Alfa Aesar). Their quantity was adjusted to reach a predefined theoretical molar coordination ratio:

$$Coordination\ ratio = \frac{n_{Zn}}{n_{COOH(citric\ acid+CMC)}} \quad (5)$$

Note that 0.9 and 3 COOH are considered per CMC monomer and CA molecule, respectively (the molecules scheme is available in Figure S7e). Another buffer molecule which is not complexing towards metals was also used instead of citric acid, namely piperazine-N,N′-*bis*(3-propanesulfonic acid) (≥ 97%; Millipore).

Electrodes

The Si powder used as active material was obtained by ball-milling commercial Si powder (325 mesh, 99.96%; Materion) using a HD-01 attritor (Union Process). The milling was performed under argon atmosphere for 20 h at 600 rpm with a ball-to-powder mass ratio of 10:1. The as-milled Si powder was composed of micrometric agglomerates as primary particles ($d_{50} \approx$ 10 µm, $S_{BET} \approx 20$ $m^2.g^{-1}$) and secondary particles were under 1 micron. The oxygen content determined by a LECO analyzer was approximately 1 $_w$%.

160 mg of Si powder, 24 mg of graphene platelets used as conductive additive (xGnP M15 grade from XGSciences, average thickness ≈ 7 nm, average diameter = 15 µm, surface area ≈ 120-150 $m^2.g^{-1}$, according to supplier data) and 0.8 mL of binder solution (by weight) were set in a vial with three balls (d = 9.5 mm), both made of silicon nitride. The whole was mixed using a Pulverisette 7 (Fritsch) planetary mixer for 1 h at 500 rpm. Then, the as-prepared ink was tape casted with a doctor blade on a Cu foil (99.9%, thickness ≈ 20 µm, cold rolled; PI-KEM). The blade gap was h = 150 µm (model 3540, s = 5.6 $mm.s^{-1}$; Elcometer). As-prepared films were dried at room temperature for 12 h. Finally, electrodes were punched (diam. = 1 cm) and dried 2 h at 100 °C under vacuum (P ≈ 10 mbar), prior to mass (Δm = ± 0.01 mg; OHAUS), and their thicknesses (Δe = ±1 µm; Mitutoyo) were measured. Then, they were dried again for 1 h under the same conditions prior to assembly. Electrodes were selected if their active mass loading reached 1.75 ± 0.1 $mg_{Si}.cm^{-2}$. Other silicon loadings were also targeted for specific characterization such as scratch tests and STEM-EDX analysis. For the latter, electrodes with a silicon loading equal to 1.0 ± 0.1 $mg_{Si}.cm^{-2}$ were prepared following the same protocol (blade gap was h = 100 µm model 3540, s = 5.6 $mm.s^{-1}$; Elcometer).

Material characterization

Electrochemistry

Electrodes were assembled in Swagelok cells in Ar filled glove box (O_2 and H_2O < 1 ppm) in half-cell configuration. A metallic Li disc (diam. = 10 mm, thickness = 380 µm, 99.9%; Aldrich) placed on a Cu current collector (diam. = 12 mm, thickness = 250 µm) served as both counter and reference electrodes. Two layers of glass microfiber membranes were used as separator (grade GF/D, diam. = 13 mm, thickness = 670 µm; Whatman). An extra monolayer of polypropylene (PP) separator in contact with the Si electrode (grade 2500, d = 13 mm; Celgard) was used for every electrode subjected to post-mortem analysis. As such, electrodes were protected from fiber inclusion coming from GF/D separators. The separator layers were soaked with 300 µL of electrolyte made of 1 M $LiPF_6$ in ethylene carbonate (EC) and dimethyl carbonate (DMC) (1:1, v:v) plus 10 $_w$% of fluoroethylene carbonate (FEC) (99.9%; Solvionic). Si electrodes were used for the cycling tests performed at room temperature using a multichannel VMP system (Biologic) in galvanostatic mode between 0.005 to 1 V (*vs.* Li^+/Li^0). The C rate was C/40 for the 1st cycle, C/20 for the next 5 cycles and C/10 for the subsequent cycles (1C = 3820 $mA.g_{Si}^{-1}$). Prior to cycling, cells were rested 2 h at open circuit voltage (OCV). This period was set to 8 h for cells containing the extra PP layer in the separator (because of wetting issue with the DMC of the electrolyte blend). Cells were also relaxed at OCV for 10 s and 1 min after each discharge (lithiation) and charge step, respectively. For the sake of reproducibility, three to four cells were tested for each Si electrode formulation and the results were averaged.

The cycling procedure of the ZnO (0.22) containing electrode used for the STEM-EDX and ^{7}Li and ^{19}F NMR quantifications, can be found in our previous publication.[19]

IR spectroscopy

Binder IR spectra were acquired with a thermoregulated ATR 7600 spectrometer (Thermo Nicolet). Typical binder solutions were prepared either with ultra-pure water or with deuterated water when indicated. First, a drop of binder solution was set to dry for 15 minutes on the ATR diamond at 60 °C. Then, the temperature was increased to 100 °C and held. IR spectra were continuously acquired with a resolution of 4 and 2 cm^{-1} and averaged over 30 and 100 scans for the H_2O and D_2O solutions respectively. A background was acquired at 60 °C without binder and no baseline correction was applied to the sample spectra. ATR correction was applied for spectrum acquisition.

Rheology

Binder solutions and ink flow properties were determined with a MCR101 (Anton Paar) rheometer. The geometry used was cone-plane (d = 50 mm, h = 46 µm, angle ≈ 0.984 °) and plane-plane (d = 50 mm, h = 300 µm) for solutions and inks, respectively. Temperature was regulated to 20 °C with a Peltier probe. Binder solutions were magnetically stirred for 1 h at 300 rpm and then rested at least 30 minutes to set the same work history whereas inks were used as prepared. Storage (G') and loss (G'') modulus were measured with increasing strain from 0.01 to 100% at a frequency of 1 Hz. Shear stress and viscosity were measured with increasing shear rate from 0.01 to 1000 s^{-1} and then down again to 0.01 s^{-1}. Binder viscosities are taken on the forward scan and the back scan was used to evaluate any thixotropic behavior.[28] However, back scan ink viscosities are presented as tape casting occurs after the high-shear planetary mixing step.

STEM-EDX

Scanning transmission electron microscopy (STEM) experiments were carried out using the Nant'Themis, a (S)TEM Themis Z G3 Cs-probe corrected microscope (Thermo Fisher Scientific) operated at 80 kV and equipped with a high-angle annular dark field (HAADF) detector. Elemental maps were acquired in STEM mode using a Super-X emission X-ray spectrometer consisting of four windowless silicon-drift detectors (SDDs) providing a large collection solid angle of 0.7 srad. For the electrodes to be measured, this configuration ensured a limited sensitivity to the aggregate orientations with respect to the detectors. In order to limit electron beam degradation effects often observed on Si-based electrodes,[69] a small convergence angle of around 13 mrad and limited current of 100 pA were used, thus reducing the electron dose. For this same reason, fast frame acquisitions were used (couple of seconds per frame and 10-50 µs dwell time) and hundreds of frames summed for each map. Pixel sizes of approximately 5 nm were chosen. Quantifications performed on the first dozens of frames gave very similar results to those performed on the last dozens of frames, thus proving the reliability of given atomic ratios and maps. Regions purely composed of LiF were nevertheless slightly degraded in these conditions, without major implications on the relevance of the maps presented here. Thanks to a 5 eV/channel value for energy dispersion, light elements could be reliably measured.

Pristine electrodes (without *x*GnPM15) powder was dispersed in cyclohexane after being scratched from the current collector. Then, a drop was deposited onto a lacey carbon film supported by a copper grid. ZnO (0.22) containing electrode powder with a silicon loading of 1.0 ± 0.1 $mg_{Si}.cm^{-2}$ was deposited onto a lacey carbon film by simple contact of the powder with the

copper grid. After one cycle, the electrodes were not rinsed and further dried at T = 40 °C, t = 20 h, P ≈ 1 mbar without air exposure, then scratched from the current collector. A vacuum transfer sample holder (GATAN 648) was used to prevent any air contact of the reactive sample before its introduction into the Nant'Themis.

Scratch test

Electrodes coating adhesion and cohesion properties were determined using a sclerometer (BYK-Gardner). First, coatings were cut in the dimension of microscope slides (26 x 76 mm). Then, they were dried, weighted and measured (for the thickness) in the same way as the electrodes. Samples were taped on the slides such that the scratches were normal to the electrode tape casting direction. Thus, each scratch passed through an approximately equivalent thickness. The stylus (d = 1.9 mm, angle = 60 °, d_{tip} = 150 µm; BYK) was set on the coating and loaded with masses. Then, the plate was moved (s = 336 $mm.min^{-1}$) to make the scratch. Finally, scratches were analyzed with an SDD (SAMx) EDX probe in a 5800LV (Jeol) SEM with a gun voltage and current of 15 kV and 0.5 nA, respectively.

Indentation

Electrode coating mechanical properties were analyzed using a nano-indenter NHT^3 and a MicroCombi MCT^3 (Anton Paar). The former can couple a sinusoidal load to the standard one to render a hardness and elastic modulus depth profile. Electrodes were dried at 100 °C and 10 mbar for 1 h, to mimic battery conditions. The head (Berkovich) applied a maximum force of 0.1 to 400 mN. The oscillating contribution amplitude was 5% of the force at any moment and a frequency of 5 Hz and an acceleration coefficient (CSR strength ramp) of 0.1 s^{-1} were used. For

the micro-indenter (Vickers), the depth profile was obtained by applying quasi-static loads. The load intensity was increased 10 times, from 30 mN to 1 N, and was maintained for 15 s every time. The loading/unloading time was 15 s. The Oliver and Pharr[70] method was used to determine the hardness and elastic modulus. For the latter calculus, the Poisson coefficient was postulated to be 0.3. Finally, the mechanical properties were evaluated under battery operation conditions. To do so, the electrodes were soaked for 10 min in propylene carbonate (PC) and the surplus was removed before testing.

Operando dilatometry

Electrode thickness variation was monitored *operando* using an ECD-2 (El-cell) coupled dilatometric and a three electrode cycling cell whose scheme has been published elsewhere.[63] The thickness variation was measured with a LVDT sensor with a resolution of 0.05 µm. The counter electrode was metallic Li (d = 16mm, thickness = 750 µm, 99.9%; Fisher). A lithium reference electrode was set in contact with porous sintered glass which was used as separator (thickness = 6 mm). The electrolyte (V ≈ 2 mL) and working electrode were the same as for the Swagelok cells. The only exception was the Cu current collector (thickness = 120 µm, annealed, 99.9%; Alfa Aesar). Cycling conditions were also identical except for the OCV period, which was set to 12 h for the cell linear drift calculus and correction. Some electrodes were also limited with a 1200 $mAh.g_{Si}^{-1}$ cutoff.

NMR spectroscopy

Solid state magic angle spinning nuclear magnetic resonance (MAS NMR) spectra were acquired for Si and binder blends prepared the same way as the electrodes but without graphite

and tape casted on Mylar (dried at 100 °C and 10 mbar for 1 h, to mimic battery conditions.). This was necessary to avoid any diffusion of paramagnetic Cu(II) in the electrode that would originate from the Cu current collector oxidation.[15] Additional analyses were also performed on reference compounds and starting binder materials (dried at 60 °C). ^{13}C and ^{17}O NMR spectra were acquired on a 500 MHz Bruker Avance III spectrometer using 4mm and 2.5 mm Bruker MAS probes, respectively. ^{1}H-^{13}C Cross-Polarization NMR spectra were acquired with a 2 ms contact time, a MAS frequency of 11 kHz, and a recycle delay ranging from 2 to 5 s. For each acquisition, a ^{1}H TPPM15 decoupling scheme was used with a 90 kHz radiofrequency (RF) strength. ^{17}O MAS spectra were acquired with a single $\pi/12$ pulse excitation of 71 kHz RF strength. The MAS frequency was set to 27 kHz and the recycle delay to 2 s. ^{17}O signal enhancement using a Double Frequency Sweep pulse was discarded here, as we observed spectral distortion for some samples. ^{13}C and ^{17}O NMR spectra are referenced relative to TMS and H_2O, respectively.

^{7}Li and ^{19}F MAS NMR experiments were performed on a 500 MHz Bruker Avance III (Larmor Frequency $\nu_0(^{7}Li)$ = 194 MHz, $\nu_0(^{19}F)$ = 470 MHz) with zirconia rotor (d_{ext} = 2.5 mm). ^{7}Li and ^{19}F spectra were acquired using a single pulse and Hahn echo sequence and a 30, 15 s recycle delay respectively. Spinning frequencies up to 25 kHz were used. Also, long recycle times were used to ensure quantitative measurements, with all spectra normalized taking into account the number of scans, the receiver gain and the mass of the sample. ^{7}Li and ^{19}F integrated intensities were determined by using spectral simulation Dmfit software.[71] Quantitative NMR was also performed by mixing Si with various amounts of LiF to obtain calibration curves. It allowed lithium and fluorine absolute quantification in the samples.[72] The electrodes (1.00 and 1.75 ± 0.1 $mg_{Si}.cm^{-2}$) were cycled for 1 cycle, then not rinsed and further dried, T = 40 °C, t = 20

h, P ≈ 1 mbar, without air exposure. It is important to note that even if the electrodes were not rinsed, they were gently placed on an absorbent paper. It had the effect of extracting almost all the liquid electrolyte contained in the porosity. Indeed, pristine electrodes had a mass gain of less than 1%, after mimicking battery conditions for a night and following the same dismantling plus drying procedure as cycled electrodes.

ASSOCIATED CONTENT

Supporting information

Electrode dimensions and 1st cycle electrochemical performance; ^{7}Li and ^{19}F NMR quantification and STEM-EDX observation; 1st cycle dQ/dV curves centered on FEC reduction region; IR spectra and cycling performance of $Zn(NO_3)_2$ electrode; binder and ink rheology; ^{17}O and ^{13}C NMR analyses; cycling performance of PIPPS formulation; mechanical characterization (scratch test, nano/micro-indentation, operando dilatometry) supplementary information.

AUTHOR INFORMATION

Author contributions

L.H: conceptualization, investigation and writing original draft. D.M.: conceptualization and methodology. P.M.: conceptualization and STEM-EDX investigation. N.D.: conceptualization and ^{7}Li and ^{19}F NMR investigation. M.P.: ^{13}C and ^{17}O NMR investigation and writing original draft. S.M.: ^{17}O NMR investigation and writing original draft. D.L.: ^{17}O NMR investigation and writing original draft. T.D.: conceptualization, supervision and writing review and editing. L.R.: conceptualization, supervision and writing review and editing. B.L.: conceptualization, supervision and writing review and editing.

ACKNOWLEDGMENTS

Funding by the French Contrat Plan État-Région and the European Regional Development Fund of Pays de la Loire, the CIMEN Electron Microscopy Center in Nantes, and the Natural Sciences and Engineering Research Council (NSERC) of Canada (grant RGPIN-2021-03374) is greatly acknowledged. Guillaume Berthout and Jiri Nohava from Anton Parr are gratefully acknowledged for the help with the nano and micro-indentation experiments. Dr Thomas Xavier Métro (IBMM, Montpellier) is acknowledged for his contribution to the elaboration of ^{17}O-enriched citric acid. Natalie Herkendaal is gratefully acknowledged for the careful proof reading.

REFERENCES

[1] H. Chen, M. Ling, L. Hencz, H.Y. Ling, G. Li, Z. Lin, G. Liu, S. Zhang, Exploring Chemical, Mechanical, and Electrical Functionalities of Binders for Advanced Energy-Storage Devices, Chem. Rev. 118 (2018) 8936–8982. https://doi.org/10.1021/acs.chemrev.8b00241.

[2] A. Miranda, K. Sarang, B. Gendensuren, E.-S. Oh, J. Lutkenhaus, R. Verduzco, Molecular design principles for polymeric binders in silicon anodes, Mol. Syst. Des. Eng. 5 (2020) 709–724. https://doi.org/10.1039/C9ME00162J.

[3] S. Li, Y.-M. Liu, Y.-C. Zhang, Y. Song, G.-K. Wang, Y.-X. Liu, Z.-G. Wu, B.-H. Zhong, Y.-J. Zhong, X.-D. Guo, A review of rational design and investigation of binders applied in silicon-based anodes for lithium-ion batteries, J. Power Sources. 485 (2021) 229331. https://doi.org/10.1016/j.jpowsour.2020.229331.

[4] H. Wang, B. Wu, X. Wu, Q. Zhuang, T. Liu, Y. Pan, G. Shi, H. Yi, P. Xu, Z. Xiong, S.-L. Chou, B. Wang, Key Factors for Binders to Enhance the Electrochemical Performance of Silicon Anodes through Molecular Design, Small. 18 (2022) 2101680. https://doi.org/10.1002/smll.202101680.

[5] A.N. Preman, H. Lee, J. Yoo, I.T. Kim, T. Saito, S. Ahn, Progress of 3D network binders in silicon anodes for lithium ion batteries, J. Mater. Chem. A. 8 (2020) 25548–25570. https://doi.org/10.1039/D0TA07713E.

[6] Z. Chen, H. Zhang, T. Dong, P. Mu, X. Rong, Z. Li, Uncovering the Chemistry of Cross-Linked Polymer Binders via Chemical Bonds for Silicon-Based Electrodes, ACS Appl. Mater. Interfaces. 12 (2020) 47164–47180. https://doi.org/10.1021/acsami.0c12519.

[7] T. Kwon, J.W. Choi, A. Coskun, The emerging era of supramolecular polymeric binders in silicon anodes, Chem. Soc. Rev. 47 (2018) 2145–2164. https://doi.org/10.1039/C7CS00858A.

[8] J. Liu, Q. Zhang, Z.-Y. Wu, J.-H. Wu, J.-T. Li, L. Huang, S.-G. Sun, A high-performance alginate hydrogel binder for the Si/C anode of a Li-ion battery, Chem. Commun. 50 (2014) 6386–6389. https://doi.org/10.1039/C4CC00081A.

[9] J. Yoon, D.X. Oh, C. Jo, J. Lee, D.S. Hwang, Improvement of desolvation and resilience of alginate binders for Si-based anodes in a lithium ion battery by calcium-mediated cross-linking, Phys Chem Chem Phys. 16 (2014) 25628–25635. https://doi.org/10.1039/C4CP03499F.

[10] L. Zhang, L. Zhang, L. Chai, P. Xue, W. Hao, H. Zheng, A coordinatively cross-linked polymeric network as a functional binder for high-performance silicon submicro-particle

anodes in lithium-ion batteries, J Mater Chem A. 2 (2014) 19036–19045. https://doi.org/10.1039/C4TA04320K.

[11] Z.-Y. Wu, L. Deng, J.-T. Li, Q.-S. Huang, Y.-Q. Lu, J. Liu, T. Zhang, L. Huang, S.-G. Sun, Multiple hydrogel alginate binders for Si anodes of lithium-ion battery, Electrochimica Acta. 245 (2017) 371–378. https://doi.org/10.1016/j.electacta.2017.05.094.

[12] Y. Gu, S. Yang, G. Zhu, Y. Yuan, Q. Qu, Y. Wang, H. Zheng, The effects of cross-linking cations on the electrochemical behavior of silicon anodes with alginate binder, Electrochimica Acta. 269 (2018) 405–414. https://doi.org/10.1016/j.electacta.2018.02.168.

[13] B. Gendensuren, E.-S. Oh, Dual-crosslinked network binder of alginate with polyacrylamide for silicon/graphite anodes of lithium ion battery, J. Power Sources. 384 (2018) 379–386. https://doi.org/10.1016/j.jpowsour.2018.03.009.

[14] C.R. Hernandez, A. Etiemble, T. Douillard, D. Mazouzi, Z. Karkar, E. Maire, D. Guyomard, B. Lestriez, L. Roué, A Facile and Very Effective Method to Enhance the Mechanical Strength and the Cyclability of Si-Based Electrodes for Li-Ion Batteries, Adv. Energy Mater. 8 (2018) 1701787. https://doi.org/10.1002/aenm.201701787.

[15] D. Mazouzi, R. Grissa, M. Paris, Z. Karkar, L. Huet, D. Guyomard, L. Roué, T. Devic, B. Lestriez, CMC-citric acid Cu(II) cross-linked binder approach to improve the electrochemical performance of Si-based electrodes, Electrochimica Acta. 304 (2019) 495–504. https://doi.org/10.1016/j.electacta.2019.03.026.

[16] Y.K. Jeong, J.W. Choi, Mussel-Inspired Self-Healing Metallopolymers for Silicon Nanoparticle Anodes, ACS Nano. 13 (2019) 8364–8373. https://doi.org/10.1021/acsnano.9b03837.

[17] J. Kim, K. Park, Y. Cho, H. Shin, S. Kim, K. Char, J.W. Choi, Zn^{2+} –Imidazole Coordination Crosslinks for Elastic Polymeric Binders in High- Capacity Silicon Electrodes, Adv. Sci. 8 (2021) 2004290. https://doi.org/10.1002/advs.202004290.

[18] T. Devic, B. Lestriez, L. Roué, Silicon Electrodes for Li-Ion Batteries. Addressing the Challenges through Coordination Chemistry, ACS Energy Lett. 4 (2019) 550–557. https://doi.org/10.1021/acsenergylett.8b02433.

[19] L. Huet, P. Moreau, N. Dupré, T. Devic, L. Roué, B. Lestriez, Nanoscale Morphological Characterization of Coordinated Binder and Solid Electrolyte Interphase in Silicon- Based Electrodes for Li- Ion Batteries, Small Methods. (2022) 2200827. https://doi.org/10.1002/smtd.202200827.

[20] Z. Karkar, D. Guyomard, L. Roué, B. Lestriez, A comparative study of polyacrylic acid (PAA) and carboxymethyl cellulose (CMC) binders for Si-based electrodes, Electrochimica Acta. 258 (2017) 453–466. https://doi.org/10.1016/j.electacta.2017.11.082.

[21] J. Xiong, N. Dupré, D. Mazouzi, D. Guyomard, L. Roué, B. Lestriez, Influence of the Polyacrylic Acid Binder Neutralization Degree on the Initial Electrochemical Behavior of a Silicon/Graphite Electrode, ACS Appl. Mater. Interfaces. 13 (2021) 28304–28323. https://doi.org/10.1021/acsami.1c06683.

[22] J. Shin, T.-H. Kim, Y. Lee, E. Cho, Key functional groups defining the formation of Si anode solid-electrolyte interphase towards high energy density Li-ion batteries, Energy Storage Mater. 25 (2020) 764–781. https://doi.org/10.1016/j.ensm.2019.09.009.

[23] C.C. Nguyen, T. Yoon, D.M. Seo, P. Guduru, B.L. Lucht, Systematic Investigation of Binders for Silicon Anodes: Interactions of Binder with Silicon Particles and Electrolytes

and Effects of Binders on Solid Electrolyte Interphase Formation, ACS Appl. Mater. Interfaces. 8 (2016) 12211–12220. https://doi.org/10.1021/acsami.6b03357.

[24] S. Yang, Y. Gu, Q. Qu, G. Zhu, G. Liu, V.S. Battaglia, H. Zheng, Engineered Si@alginate microcapsule-graphite composite electrode for next generation high-performance lithium-ion batteries, Electrochimica Acta. 270 (2018) 480–489. https://doi.org/10.1016/j.electacta.2018.03.039.

[25] Y. Jin, N.-J.H. Kneusels, L.E. Marbella, E. Castillo-Martínez, P.C.M.M. Magusin, R.S. Weatherup, E. Jónsson, T. Liu, S. Paul, C.P. Grey, Understanding Fluoroethylene Carbonate and Vinylene Carbonate Based Electrolytes for Si Anodes in Lithium Ion Batteries with NMR Spectroscopy, J. Am. Chem. Soc. 140 (2018) 9854–9867. https://doi.org/10.1021/jacs.8b03408.

[26] Y. Jin, N.-J.H. Kneusels, P.C.M.M. Magusin, G. Kim, E. Castillo-Martínez, L.E. Marbella, R.N. Kerber, D.J. Howe, S. Paul, T. Liu, C.P. Grey, Identifying the Structural Basis for the Increased Stability of the Solid Electrolyte Interphase Formed on Silicon with the Additive Fluoroethylene Carbonate, J. Am. Chem. Soc. 139 (2017) 14992–15004. https://doi.org/10.1021/jacs.7b06834.

[27] C.G. Lopez, S.E. Rogers, R.H. Colby, P. Graham, J.T. Cabral, Structure of sodium carboxymethyl cellulose aqueous solutions: A SANS and rheology study, J. Polym. Sci. Part B Polym. Phys. 53 (2015) 492–501. https://doi.org/10.1002/polb.23657.

[28] C.G. Lopez, R.H. Colby, J.T. Cabral, Electrostatic and Hydrophobic Interactions in NaCMC Aqueous Solutions: Effect of Degree of Substitution, Macromolecules. 51 (2018) 3165–3175. https://doi.org/10.1021/acs.macromol.8b00178.

[29] C.G. Lopez, Entanglement of semiflexible polyelectrolytes: Crossover concentrations and entanglement density of sodium carboxymethyl cellulose, J. Rheol. 64 (2020) 191–204. https://doi.org/10.1122/1.5127015.

[30] C.G. Lopez, W. Richtering, Oscillatory rheology of carboxymethyl cellulose gels: Influence of concentration and pH, Carbohydr. Polym. 267 (2021) 118117. https://doi.org/10.1016/j.carbpol.2021.118117.

[31] W.N. Sharratt, R. O'Connell, S.E. Rogers, C.G. Lopez, J.T. Cabral, Conformation and Phase Behavior of Sodium Carboxymethyl Cellulose in the Presence of Mono- and Divalent Salts, Macromolecules. 53 (2020) 1451–1463. https://doi.org/10.1021/acs.macromol.9b02228.

[32] C.G. Lopez, R.H. Colby, P. Graham, J.T. Cabral, Viscosity and Scaling of Semiflexible Polyelectrolyte NaCMC in Aqueous Salt Solutions, Macromolecules. 50 (2017) 332–338. https://doi.org/10.1021/acs.macromol.6b02261.

[33] C.G. Lopez, W. Richtering, Influence of divalent counterions on the solution rheology and supramolecular aggregation of carboxymethyl cellulose, Cellulose. 26 (2019) 1517–1534. https://doi.org/10.1007/s10570-018-2158-8.

[34] T. Budtova, P. Navard, Cellulose in NaOH–water based solvents: a review, Cellulose. 23 (2016) 5–55. https://doi.org/10.1007/s10570-015-0779-8.

[35] C.G. Lopez, Entanglement Properties of Polyelectrolytes in Salt-Free and Excess-Salt Solutions, ACS Macro Lett. 8 (2019) 979–983. https://doi.org/10.1021/acsmacrolett.9b00161.

[36] A.A. Sheikh-Osman, R. Bertani, A. Tapparo, G.G. Bombi, B. Corain, Aluminium carboxylates in aqueous solutions. Part 3. Synthesis and solution state of

[Al2(cit)2(H2O)6], [Al2(tart)3(H2O)4] and [Al(gluc)(OH)2](H3cit = citric acid, H2tart = tartaric acid, Hgluc = gluconic acid), J. Chem. Soc. Dalton Trans. (1993) 3229–3233. https://doi.org/10.1039/DT9930003229.

[37] S. Jaiser, J. Kumberg, J. Klaver, J.L. Urai, W. Schabel, J. Schmatz, P. Scharfer, Microstructure formation of lithium-ion battery electrodes during drying – An ex-situ study using cryogenic broad ion beam slope-cutting and scanning electron microscopy (Cryo-BIB-SEM), J. Power Sources. 345 (2017) 97–107. https://doi.org/10.1016/j.jpowsour.2017.01.117.

[38] O.D. Bonner, J.D. Curry, Infrared spectra of liquid H_2O and D_2O, Infra. Phys. 10 (1970) 91-94.

[39] S. Toda, A. Sakai, Y. Kojima, On the infrared absorption spectra of zinc stearate complex, Spectrochim. Acta Part A 27 (1971) 581-592.

[40] K.I. Hadjiivanov, D.A. Panayotov, M.Y. Mihaylov, E.Z. Ivanova, K.K. Chakarova, S.M. Andonova, N.L. Drenchev, Power of Infrared and Raman Spectroscopies to Characterize Metal-Organic Frameworks and Investigate Their Interaction with Guest Molecules, Chem. Rev. 121 (2021) 1286–1424. https://doi.org/10.1021/acs.chemrev.0c00487.

[41] G. Wu, 17O NMR studies of organic and biological molecules in aqueous solution and in the solid state, Prog. Nucl. Magn. Reson. Spectrosc. 114–115 (2019) 135–191. https://doi.org/10.1016/j.pnmrs.2019.06.002.

[42] J. Špačková, C. Fabra, G. Cazals, M. Hubert-Roux, I. Schmitz-Afonso, I. Goldberga, D. Berthomieu, A. Lebrun, T.-X. Métro, D. Laurencin, Cost-efficient and user-friendly ^{17}O/ ^{18}O labeling procedures of fatty acids using mechanochemistry, Chem. Commun. 57 (2021) 6812–6815. https://doi.org/10.1039/D1CC02165F.

[43] P. Che, D. Fang, D. Zhang, J. Feng, J. Wang, N. Hu, J. Meng, Hydrothermal synthesis and crystal structure of a new two-dimensional zinc citrate complex, J. Coord. Chem. 58 (2005) 1581–1588. https://doi.org/10.1080/00958970500244112.

[44] C. Leroy, T.-X. Métro, I. Hung, Z. Gan, C. Gervais, D. Laurencin, From *Operando* Raman Mechanochemistry to "NMR Crystallography": Understanding the Structures and Interconversion of Zn-Terephthalate Networks Using Selective ^{17} O-Labeling, Chem. Mater. 34 (2022) 2292–2312. https://doi.org/10.1021/acs.chemmater.1c04132.

[45] C.C. Nguyen, D.M. Seo, K.W.D.K. Chandrasiri, B.L. Lucht, Improved Cycling Performance of a Si Nanoparticle Anode Utilizing Citric Acid as a Surface-Modifying Agent, Langmuir. 33 (2017) 9254–9261. https://doi.org/10.1021/acs.langmuir.6b04310.

[46] K.W.D.K. Chandrasiri, C.C. Nguyen, B.S. Parimalam, S. Jurng, B.L. Lucht, Citric Acid Based Pre-SEI for Improvement of Silicon Electrodes in Lithium Ion Batteries, J. Electrochem. Soc. 165 (2018) A1991–A1996. https://doi.org/10.1149/2.0161810jes.

[47] A.M. Gaikwad, A.C. Arias, Understanding the Effects of Electrode Formulation on the Mechanical Strength of Composite Electrodes for Flexible Batteries, ACS Appl. Mater. Interfaces. 9 (2017) 6390–6400. https://doi.org/10.1021/acsami.6b14719.

[48] D. Mazouzi, B. Lestriez, L. Roué, D. Guyomard, Silicon Composite Electrode with High Capacity and Long Cycle Life, Electrochem. Solid-State Lett. 12 (2009) A215. https://doi.org/10.1149/1.3212894.

[49] N. Delpuech, D. Mazouzi, N. Dupré, P. Moreau, M. Cerbelaud, J.S. Bridel, J.-C. Badot, E. De Vito, D. Guyomard, B. Lestriez, B. Humbert, Critical Role of Silicon Nanoparticles Surface on Lithium Cell Electrochemical Performance Analyzed by FTIR, Raman, EELS,

XPS, NMR, and BDS Spectroscopies, J. Phys. Chem. C. 118 (2014) 17318–17331. https://doi.org/10.1021/jp503949y.

[50] F. Jeschull, F. Scott, S. Trabesinger, Interactions of silicon nanoparticles with carboxymethyl cellulose and carboxylic acids in negative electrodes of lithium-ion batteries, J. Power Sources. 431 (2019) 63–74. https://doi.org/10.1016/j.jpowsour.2019.05.036.

[51] A. Roland, B. Delarre, J.-B. Ledeuil, N. Louvain, H. Martinez, L. Monconduit, Silicon-based electrodes formulation in buffered solution for enhanced electrode-electrolyte interfaces, J. Power Sources. 489 (2021) 229465. https://doi.org/10.1016/j.jpowsour.2021.229465.

[52] Y. Wang, D. Dang, D. Li, J. Hu, Y.-T. Cheng, Influence of polymeric binders on mechanical properties and microstructure evolution of silicon composite electrodes during electrochemical cycling, J. Power Sources. 425 (2019) 170–178. https://doi.org/10.1016/j.jpowsour.2019.04.006.

[53] F. Jeschull, M.J. Lacey, D. Brandell, Functional binders as graphite exfoliation suppressants in aggressive electrolytes for lithium-ion batteries, Electrochimica Acta. 175 (2015) 141–150. https://doi.org/10.1016/j.electacta.2015.03.072.

[54] Z. Zhang, T. Zeng, Y. Lai, M. Jia, J. Li, A comparative study of different binders and their effects on electrochemical properties of LiMn 2 O 4 cathode in lithium ion batteries, J. Power Sources. 247 (2014) 1–8. https://doi.org/10.1016/j.jpowsour.2013.08.051.

[55] A. Magasinski, B. Zdyrko, I. Kovalenko, B. Hertzberg, R. Burtovyy, C.F. Huebner, T.F. Fuller, I. Luzinov, G. Yushin, Toward Efficient Binders for Li-Ion Battery Si-Based

Anodes: Polyacrylic Acid, ACS Appl. Mater. Interfaces. 2 (2010) 3004–3010. https://doi.org/10.1021/am100871y.

[56] A. Tranchot, H. Idrissi, P.-X. Thivel, L. Roué, Influence of the Si particle size on the mechanical stability of Si-based electrodes evaluated by in-operando dilatometry and acoustic emission, J. Power Sources. 330 (2016) 253–260. https://doi.org/10.1016/j.jpowsour.2016.09.017.

[57] Z. Karkar, T. Jaouhari, A. Tranchot, D. Mazouzi, D. Guyomard, B. Lestriez, L. Roué, How silicon electrodes can be calendered without altering their mechanical strength and cycle life, J. Power Sources. 371 (2017) 136–147. https://doi.org/10.1016/j.jpowsour.2017.10.042.

[58] M.N. Obrovac, L.J. Krause, Reversible Cycling of Crystalline Silicon Powder, J. Electrochem. Soc. 154 (2007) A103. https://doi.org/10.1149/1.2402112.

[59] Z. Du, R.A. Dunlap, M.N. Obrovac, High Energy Density Calendered Si Alloy/Graphite Anodes, J. Electrochem. Soc. 161 (2014) A1698–A1705. https://doi.org/10.1149/2.0941410jes.

[60] J.W. Hutchinson, Z. Suo, Mixed Mode Cracking in Layered Materials, in: Adv. Appl. Mech., Elsevier, 1991: pp. 63–191. https://doi.org/10.1016/S0065-2156(08)70164-9.

[61] M.D. Thouless, J.W. Hutchinson, E.G. Liniger, Plane-strain, buckling-driven delamination of thin films: Model experiments and mode-II fracture, Acta Metall. Mater. 40 (1992) 2639–2649. https://doi.org/10.1016/0956-7151(92)90333-A.

[62] M.N. Obrovac, V.L. Chevrier, Alloy Negative Electrodes for Li-Ion Batteries, Chem. Rev. 114 (2014) 11444–11502. https://doi.org/10.1021/cr500207g.

[63] A. Tranchot, H. Idrissi, P.X. Thivel, L. Roué, Impact of the Slurry pH on the Expansion/Contraction Behavior of Silicon/Carbon/Carboxymethylcellulose Electrodes for Li-Ion Batteries, J. Electrochem. Soc. 163 (2016) A1020–A1026. https://doi.org/10.1149/2.1071606jes.

[64] X. Zhang, S. Weng, G. Yang, Y. Li, H. Li, D. Su, L. Gu, Z. Wang, X. Wang, L. Chen, Interplay between solid-electrolyte interphase and (in)active LixSi in silicon anode, Cell Rep. Phys. Sci. 2 (2021) 100668. https://doi.org/10.1016/j.xcrp.2021.100668.

[65] Z. Karkar, D. Mazouzi, C.R. Hernandez, D. Guyomard, L. Roué, B. Lestriez, Threshold-like dependence of silicon-based electrode performance on active mass loading and nature of carbon conductive additive, Electrochimica Acta. 215 (2016) 276–288. https://doi.org/10.1016/j.electacta.2016.08.118.

[66] J. Asenbauer, M. Kuenzel, T. Eisenmann, A. Birrozzi, J.-K. Chang, S. Passerini, D. Bresser, Determination of the Volume Changes Occurring for Conversion/Alloying-Type Li-Ion Anodes upon Lithiation/Delithiation, J. Phys. Chem. Lett. 11 (2020) 8238–8245. https://doi.org/10.1021/acs.jpclett.0c02198.

[67] D.-H. Yoon, M. Marinaro, P. Axmann, M. Wohlfahrt-Mehrens, Study of the Binder Influence on Expansion/Contraction Behavior of Silicon Alloy Negative Electrodes for Lithium-Ion Batteries, J. Electrochem. Soc. 167 (2020) 160537. https://doi.org/10.1149/1945-7111/abcf4f.

[68] J.L. Gómez Cámer, J. Morales, L. Sánchez, P. Ruch, S.H. Ng, R. Kötz, P. Novák, Nanosized Si/cellulose fiber/carbon composites as high capacity anodes for lithium-ion batteries: A galvanostatic and dilatometric study, Electrochimica Acta. 54 (2009) 6713–6717. https://doi.org/10.1016/j.electacta.2009.06.085.

[69] M. Boniface, L. Quazuguel, J. Danet, D. Guyomard, P. Moreau, P. Bayle-Guillemaud, Nanoscale evolution of silicon electrodes for Li-ion batteries by low-loss STEM-EELS, Nano Lett. 16 (2016) 7381-7388.

[70] W.C. Oliver, G.M. Pharr, An improved technique for determining hardness and elastic modulus using load and displacement sensing indentation experiments, J. Mater. Res. 7 (1992) 1564–1583. https://doi.org/10.1557/JMR.1992.1564.

[71] D. Massiot, F. Fayon, M. Capron, I. King, S. Le Calvé, B. Alonso, J.-O. Durand, B. Bujoli, Z. Gan, G. Hoatson, Modelling one- and two-dimensional solid-state NMR spectra: Modelling 1D and 2D solid-state NMR spectra, Magn. Reson. Chem. 40 (2002) 70–76. https://doi.org/10.1002/mrc.984.

[72] M. Cuisinier, J.-F. Martin, P. Moreau, T. Epicier, R. Kanno, D. Guyomard, N. Dupré, Quantitative MAS NMR characterization of the LiMn1/2Ni1/2O2 electrode/electrolyte interphase, Solid State Nucl. Magn. Reson. 42 (2012) 51–61. https://doi.org/10.1016/j.ssnmr.2011.09.001.